Abstract

KING, MATTHEW RUSSELL. The Plasma Flame: Development and Application of a Hybrid Plasma at Atmospheric Pressure. (Under the direction of Dr. Jerome J. Cuomo).

The focus of this work was to develop a hybrid plasma at atmospheric pressure, which we have deemed the "plasma flame". This discharge is capable of facilitating the chemical reactivity associated with non-thermal (low energy) plasmas while operating at temperatures which can drive high energy reactions. Gas mixtures of nitrogen and oxygen were used as a model system for understanding the nature of the plasma flame. Multiple process variables and discharge characteristics were studied—gas composition, applied power, driving frequency, electron density, gas temperature, plasma temperature, radical chemistry, and reaction kinetics. It was found that this discharge produces a significant amount of nitrogen dioxide (NO_2)—over 10^{17} cm^{-3}. The production of NO_2 was found to depend predominately on the temperature differential between the plasma and ambient gas. The extent to which the NO_2-forming reactions proceed also depends on the availability of atomic oxygen (O) and nitric oxide (NO). Given the level of NO_2 formation in the plasma flame, a process was created for synthesizing nitric acid (HNO_3) we call "Acid on Demand". This process was then developed for application to the production of bioethanol and printed circuit boards (PCB's). Furthermore, the formation of syngas ($CO + H_2$) was also produced by introducing a different chemical system into the plasma flame (i.e. $CH_4 + H_2O$).

This thesis establishes a framework for understanding the complex chemistries associated with the plasma flame. Such knowledge can be extended to a number of chemical systems and potential applications. Overarching themes of this work have implications for a variety of topics, from non-equilibrium chemistry to synthesis of alternative fuels.

The Plasma Flame: Development and Application of a Hybrid Plasma at Atmospheric Pressure

by
Matthew Russell King

A thesis submitted to the Graduate Faculty of
North Carolina State University
in partial fulfillment of the
requirements for the degree of
Master of Science

Materials Science and Engineering

Raleigh, North Carolina

2009

APPROVED BY:

Dr. Joseph Tracy Assistant Professor of Materials Science	Dr. Mohamed Bourham Professor of Nuclear Engineering

Dr. Jerome J. Cuomo
Distinguished Research Professor of Materials Science
Committee Chair

Dedication

Today I stand on the shoulders of giants. This is dedicated to the tall shoulders and strong backs of all my personal giants.

Biography

Matthew King was born in Longview, TX in the year 1985. He was raised in a little town in eastern North Carolina called Pikeville, and eventually attended Charles B. Aycock High School. After graduating in 2003 he began a degree program in Materials Science and Engineering at NC State University. Two years passed in that curriculum, at which point he developed a distinct feeling that Materials Science didn't provide the perfect fit he was looking for. In the spirit of exploration (both literally and intellectually) he chose to pursue a degree in Geology, the idea at the time being "well, geology is like materials science, except with natural materials instead of synthetic ones". These were great years filled with, among many other things, cross-country trips to study geologic formations (i.e. non-stop periods of rock destruction with a rock hammer and chisel); development of an ever-growing, deep-seated love for the natural world; and opportunities to teach in a college classroom. Perhaps the most important (and fortuitous) benefit of studying geology was the freedom. Because of an extremely flexible curriculum, Matthew was able to continue taking classes in Materials Science, as well as other courses which piqued his curiosity. He was also able, through no skill of his own, to find a job as a lab assistant with Dr. Jerry Cuomo. Even though he was truly raised in eastern North Carolina, Dr. Cuomo's office and the halls of EB1 are where he was raised as a scientist. These years were filled with discussions on the nature of the world (even dark matter!) and many, many wonderful hours in the lab. Having found the perfect fit he was looking for, Matthew decided to come back to his home in Materials Science and

continue his exploration by going to graduate school. Fortunately for Matthew, Dr. Cuomo is a very understanding person who continued to allow the freedom he so cherished. Under the umbrella of IMST, Matthew dove into plasma science, optics, spectroscopy, chemistry, physics, statistics, and all manner of obscure papers from the early 1900's. Two years and an untold number of hours later, he emerged with a Master's Degree, a fiancé and a collection of life-changing experiences.

Acknowledgements

There are so many people without whom this thesis would have never been possible. It seems best to start with family. To Amy, who was everything I needed her to be through this process and always, I can never begin to thank you enough. You are my light and my rock!

Thank you, thank you, Mom, Dad, Christopher, Nick and Emily. Your never-ending support has made me into the person I am today, and there is no way I could have made it without you. I also have an amazing extended family and each one of them deserves my thanks (sorry I can't list everyone here; you are all listed in my heart!).

My family at the IMST was also an essential part of this work. First and foremost, my deepest gratitude goes to Dr. Cuomo, my advisor, mentor, teacher, student (*very* rarely), and confidant. Thank you for everything—I will always look back on my time with you with reverence. I will also never forget your stories! One day the kids will say, "Hey Dad, tell us another story about that crazy professor of yours!" (I mean that in the best possible way), and I will happily tell them. Thank you for allowing me to learn and letting me explore.

Thanks also go to my great friend and colleague Chris Oldham. Between his never-ending patience ("whoops, maybe I shouldn't have touched that"), deep scientific curiosity and penchant for always doing things better the next time around, I couldn't have asked to work with anyone better.

This work would also not have been possible without Dr. Dick Guarnieri's guidance and constant hassling (I mean that sincerely and in the best possible way). He always pushed me

to think about what was really going on in an experiment, and taught me that no matter what I do, I can always find a way to do it better (usually with his advice). I will never forget the importance of avoiding "operator deficiencies" and finding "clever" ways of doing things.

I would like to acknowledge Jenna Puckett for her help in this work as well. Her sharp mind was invaluable throughout this process—in both her poignant critiques and persistent suggestions.

I would also like to thank my partners-in-crime at the IMST: Brad Hartman, Jackson Thornton, Tony McWilliams, and Alderson Neira-Arce. There are few other people with whom I would have rather spent (and wasted) such massive amounts of time. You guys kept me sane, kept me sharp and above all helped me remember there is more to life than research (or so you think!). Everyone else at the IMST is also very much appreciated. Sarah Daniell, Anne Bach, Dr. Roger Sanwald, all the students and all the engineers—you all are great and I couldn't have done it without you.

Many thanks also to Dr. Simon Lappi from the Laser Laboratory in NCSU's Chemistry Department. For his advice on spectroscopy and use of the lab's equipment, I am grateful.

Finally, I would like to thank my committee members, Dr. Mohamed Bourham and Dr. Joe Tracy, for their time, their consultation and their extremely helpful (and pertinent) advice.

This work was supported by the College of Engineering and by the Department of Materials Science and Engineering. Thanks go to Dean Louis Martin-Vega and Dr. Mike Rigsbee for their support.

Table of Contents

List of Tables

List of Figures

1 Introduction

1.1 Plasmas

Plasma technologies have been around for over a century [1], and have been developed for myriad applications. In fact, plasmas have been called "the solution looking for a problem." This broad applicability stems from a number of features unique to plasmas.

At the most basic level, a plasma is an ionized gas. depending on the gas being ionized and the method used for ionization, many different environments can be created. Plasmas used for engineering applications are created by adding some form of energy to the gas of interest: electromagnetic waves (radio and microwave frequencies), electrostatic fields, high energy laser pulses (UV, visible or infrared), electron beams, or inductive coupling to name a few. Once created, the charged particles are accelerated by an electric field (either static or oscillating), and the magnitude of their energy depends partly on the magnitude of the field. It also depends on their mean free path λ, the distance between collisions with another entity, since collision events reduce the average energy of the particles. Air at room temperature has a mean free path $\lambda\,[m] = \frac{5\times10^{-5}}{p\,[Torr]}$; hence λ can vary from 500 km at ultra high vacuum (10^{-10} Torr) to 60 nm at atmospheric pressure (760 Torr). For this reason, charged species in vacuum plasmas are able to reach 10's of eV, while only ~0.1-1 eV at atmospheric pressure [2]. This is an important point; λ distinguishes very different modes of operation by facilitating differences in a wide array of plasma parameters—electron and ion energies, gas

temperature, chemical reactivity and population of energetic metastable states. The following sections will delineate commonalities of industrial plasmas and discuss key differences between conventional discharges and the one studied here. Furthermore, the relationship between plasma parameters and appropriate (or even feasible) applications will also be discussed. Lastly, the motivation for this work will be introduced in the context of matching appropriate plasma parameters to an application of interest.

1.2 Atmospheric plasmas

As mentioned earlier, the pressure and therefore the mean free path plays a dominant role in controlling plasma parameters. In vacuum, charged particles are able to gain so much energy that these plasmas are often used for thin film deposition. That is, the high energy species are accelerated into a target such that target atoms are physically removed from the surface. By changing the target material and processing variables, nearly unlimited number of materials systems can be fabricated. The electronics field has certainly benefitted from this technology, as some stage in the production of many electronic devices will undoubtedly require plasma processing.

In spite of their utility, vacuum plasmas have some drawbacks: they operate in expensive vacuum chambers and are mostly limited to batch processing. As a result, the development of uniform, controllable plasmas at atmospheric pressure has been the subject of intense investigation [1, 3-7].

1.2.1 Background on Atmospheric Plasmas

Atmospheric pressure plasmas operate in a regime in which the density of neutral species is roughly 10^{19} cm^{-3}; by comparison, at 1 mTorr it is 10^{13} cm^{-3}. This means that charged particles in an atmospheric pressure plasma have a much greater chance of colliding with a neutral gas molecule. Therefore, these particles are constantly giving up their energy as they are accelerated in the electric field, and the energy distribution is shifted to much lower energies. Since electrons have roughly 1/100,000th the mass of a molecule in air, they are accelerated to a much higher degree ($a=qE/m$) and are thus able to reach higher energies. In contrast, the heavy positive ions gain so little energy between collisions that they are usually considered at rest. This is not always the case, but it holds true for many atmospheric pressure plasmas. With electrons being accelerated to high velocities relative to the surrounding gas, an environment is created in which the energies of all species are not equal (as is the case with non-ionized gases). This is the basis of a non-equilibrium plasma.

1.2.2 Non-equilibrium Plasmas

As mentioned before, when electrons gain energy in the plasma volume and collide with heavy species—these are mostly neutrals since the ionization fraction of non-equilibrium atmospheric plasmas is relatively low—they often give up some of their energy. This interaction facilitates very specific types of excitation, and these excited modes, or "metastable" states, allow many chemical reactions to take place. In other words, high energy electrons give neutral atoms and molecules enough energy to overcome activation

barriers in chemical reactions. Furthermore, the chemical reactions can be highly inhomogeneous and restricted to only very specific excited states. This is a very advantageous situation! Most non-plasma chemical reactions rely on temperature-specific energy to drive a reaction—that is, reactions take place to a greater extent at 400°C than 300°C because the reactants have more overall energy—but since the low-mass electrons carry most of the energy, the heavy species can remain close to room temperature. Thus the term "non-thermal" is often treated as interchangeable with "non-equilibrium", even though not all non-equilibrium plasmas are non-thermal.

Now, what happens when the heavy species' temperature increases, especially to the point at which they approach the electron temperature? This creates another class of plasma, the thermal plasma.

1.2.3 Thermal Plasmas

Thermal plasmas are just that—very hot ionized gases, whose temperatures can be in the range of 10^3 – 10^6 K. These plasmas are so hot, in fact, that chemical reactions are often nonexistent. Since chemical reactions ($A+B \rightarrow C$, for example) are fundamentally based on interactions between two or more reactants, the frequency with which these reactants collide determines how thoroughly a reaction proceeds. The collision frequency is given as $\upsilon_{AB} = N_A N_B \langle \sigma v \rangle_{AB}$, where N_A and N_B are reactant concentrations, σ is the average collision cross section and v is the average velocity of the reactants. Therefore, as the temperature (i.e. velocity) of the interacting particles increases, so does the collision frequency—but only to a

certain extent. When the temperature continues to climb, the velocity increases but the collision cross section actually *decreases*. In other words, the particles are moving so fast that they are not likely to collide with one another. Thermal plasmas, then, are simply gases which have been heated using electrical energy (as opposed to conduction, convection or radiation) and have very little chemical reactivity. This property is exploited in two very common applications: welding and cutting. For these processes, the plasma's high temperature is used to melt metal.

1.2.4 Hybrid Plasmas

To summarize what has been covered in previous sections, non-equilibrium plasmas are chemically active but "cold", while thermal plasmas are very hot but have little chemical activity. Each has a range of applicability and can solve many engineering problems. There exists, however, a number of applications for which neither discharge is appropriate. These applications involve chemical systems with very large activation energies; hence, a discharge is needed which is chemically reactive (unlike thermal discharges) and can generate high gas temperatures to sustain reactions which electron collisions alone cannot facilitate (unlike non-thermal discharges). This is the realm of the hybrid discharge.

Hybrid discharges are characterized by relatively high gas temperatures (e.g. 500-5000K), but still higher electron temperatures and electron densities [8]. One very well-studied hybrid discharge is known as the "gliding arc" [9]. This discharge operates between two metal, fin-shaped electrodes. The discharge is initiated near the bottom of the fins,

where the gap is the smallest, and initially exists as a thermal discharge. It then migrates up the electrodes over time, thereby increasing the discharge volume and decreasing the temperature. In this way, the gliding arc cycles through both thermal and non-thermal regimes and is therefore capable of performing in applications listed above.

1.3 The "Plasma Flame"

The gliding arc remains one of the few (if not the only) hybrid discharges reported in the literature. As such, the goal of this work is to develop another hybrid discharge called the "plasma flame". This discharge is distinguished by the fact that it simultaneously maintains thermal and non-thermal regions and operates continuously. This becomes important when dealing with high gas flows, since the gas velocity through the reactor can approach the thermal/non-thermal transition velocity of the gliding arc.

One primary goal of this research is to develop the plasma flame for applications. As such, a chemical system was chosen on the basis of being able to establish the fundamental properties of the discharge. Operating the plasma flame in various mixtures of nitrogen and oxygen provided the necessary conditions for investigating its properties; it also allowed for investigation into the nature of that chemical system in particular. Once these things were established, the discharge was applied to problems in alternate energy, greenhouse gas reduction and microelectronics.

2 Foundations in Plasma Spectroscopy

2.1 Introduction

One of the most fundamental entities in the known universe is light. Almost everything we know about matter and energy and the origin of the universe is based on light; it also provides the energy essential for sustaining life on our planet. Soon we may even begin harnessing light to establish a completely sustainable energy grid, thereby facilitating our energy independence.

Light is also so pervasive in scientific endeavors that the study of some physical system will likely involve utilizing or measuring light. Nearly all of the brightest and most influential scientists this world has ever known at some point turned their attention to the properties of light and its interaction with matter. The list reads like a who's-who collection of influential scientists: Aristotle, Euclid, Newton, Einstein, Maxwell, Planck and Feynman, to name a few. Their work provides the foundation for many scientific endeavors, however grand or humble the scope may be.

The purpose of this chapter is to introduce the principles which lay the foundation for the work presented in the following chapters. Of particular interest are principles which allow the measurement or manipulation of light. Furthermore, methods for understanding the nature of resultant signals will be introduced for the purpose of understanding both the instrument and the system of interest. While many of the topics covered in this chapter can be applied in many different situations, the primary focus will be light-based methods in

plasma analysis. Lastly, the chapter will conclude with a brief discussion of the means by which plasmas can be classified; namely the interaction and equilibrium (or lack thereof) between electronic, vibrational, rotational and translational energies. This is a very important topic in terms of the plasma mode of operation, and it will be discussed in great detail in later chapters.

2.2 Spectrometers

A spectrometer in the most general sense is an instrument which provides a means of measuring light. The properties to be measured vary with each application but in general the metric is number of photons as a function of some parameter, e.g. wavelength, energy, time or angle of reflection.

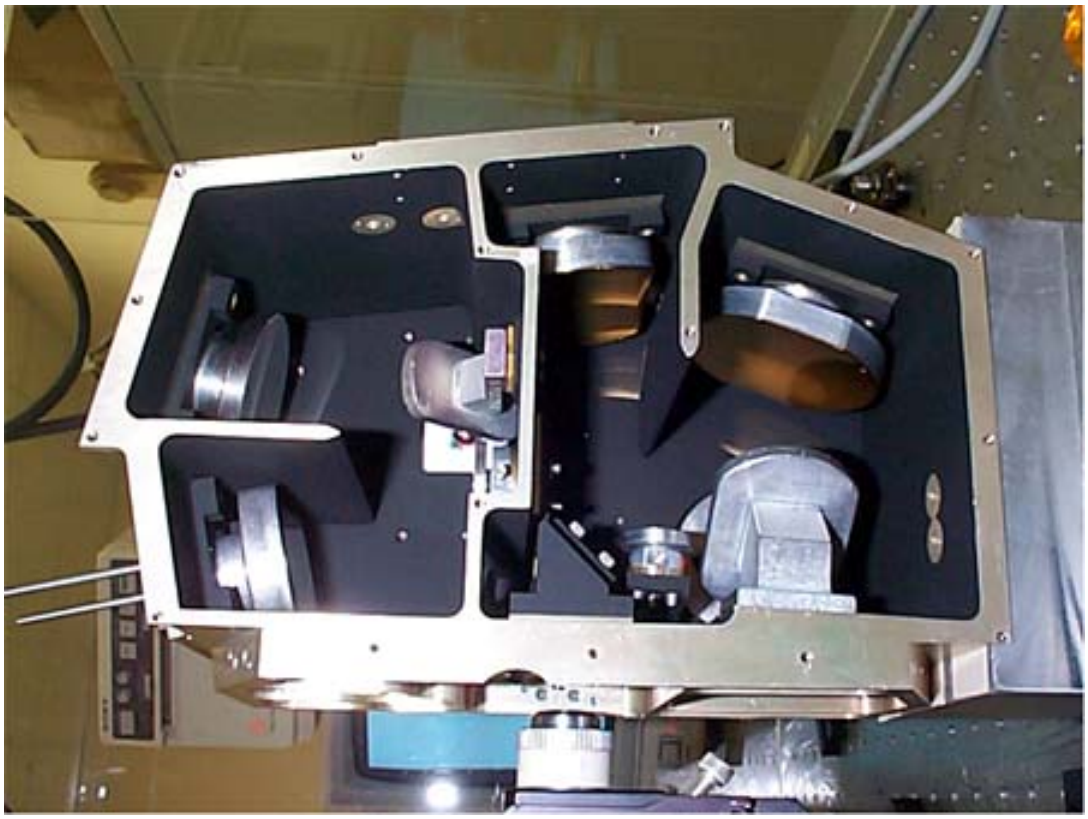

Figure 2.1. Internal components of the Compact Reconnaissance Imaging Spectrometer for Mars (CRISM), which uses spectroscopy to identify mineral deposits on the surface of Mars.

The ways in which spectrometers measure light also vary greatly. Similarities lie in the fact that all spectrometers have a few basic components: optical elements such as lenses or mirrors to control the light path into and through the spectrometer; dispersive or refractive elements which separate the continuum of polychromatic light into its component parts; and either a device which detects the light at that point or an optical element which transmits the light outside the spectrometer (Figure 2.1).

Here a distinction should be made between two common uses of these instruments: spectrometers, monochromators in particular, can be used to either detect light or facilitate the use of light for another purpose. In the case of a monochromator, the purpose is to extract a small portion of light from the input signal. The monochromatic light is then either collected with a detector or used as an illumination source, as is the case with fluorescence spectroscopy [10]. When studying plasmas, spectrometers are used to study the light emitted during processing. Optical emission studies are often broadband in nature, although monochromators are used for more advanced studies of emission lines.

To control the path of photons emitted from a plasma a number of basic optical elements are utilized. Lenses and mirrors are used for the purpose of collimating or focusing/defocusing a group of photons. Detailed discussions on basic principles of geometrical optics can be found in [11] and [12]. In addition to lenses and mirrors, another important tool is the optical fiber. These are glass fibers (SiO_2) which collect and transmit light with very little loss. Care should be taken during fiber material selection, however, as many fibers are optimized for a specific wavelength range and exhibit strong absorption in other ranges. For example a fiber with >90% transmission in the visible range may exhibit an exponential increase in absorbance at wavelengths ≤400nm. An example of this can be seen in Figure 2.2.

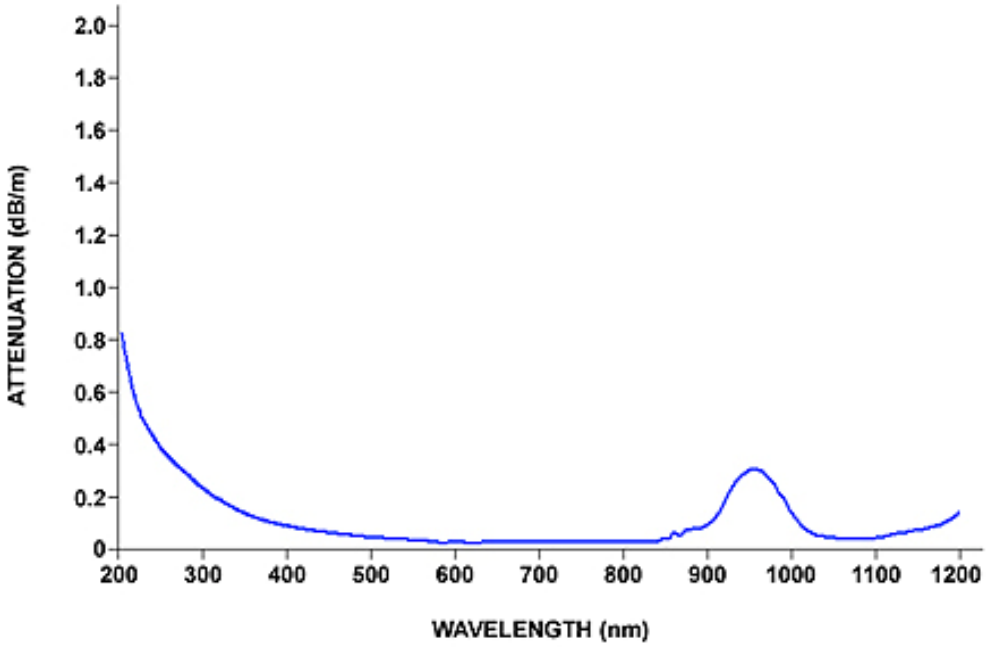

Figure 2.2. Performance of an optical fiber in the UV-Vis-IR range, from Ocean Optics, Inc.

The attenuation as a function of wavelength is shown, with the ordinate given in decibels. Since the decibel is based on a log scale, the attenuation of the fiber at wavelengths less than 400 nm represents unacceptable absorbance in the UV range. A great feature of fiber optic cables is the fact that they are flexible to a large degree, durable, and can be oriented easily in any direction. Optical fibers preclude the use of larger optical setups, wherein the orientation of mirrors and lenses must be precise and the plasma must be within the optical path of the setup.

The final optical device of interest is the heart of the spectrometer, the diffraction grating. The surface of the grating is a metal, so light incident on its surface is reflected at an angle β equal to the angle of incidence α. Gratings are based on a periodic structure of grooves,

which can have a triangular (Figure 2.3) or sinusoidal form. If the distance between grooves d is reduced to approach the wavelength λ of light being measured ($d \geq 2\lambda$) [13], the light is diffracted and orders of diffraction m begin to arise. These factors are related by the so-called grating equation, $m\lambda = d(\sin\alpha \pm \sin\beta)$, and are represented visually in Figure 2.3.

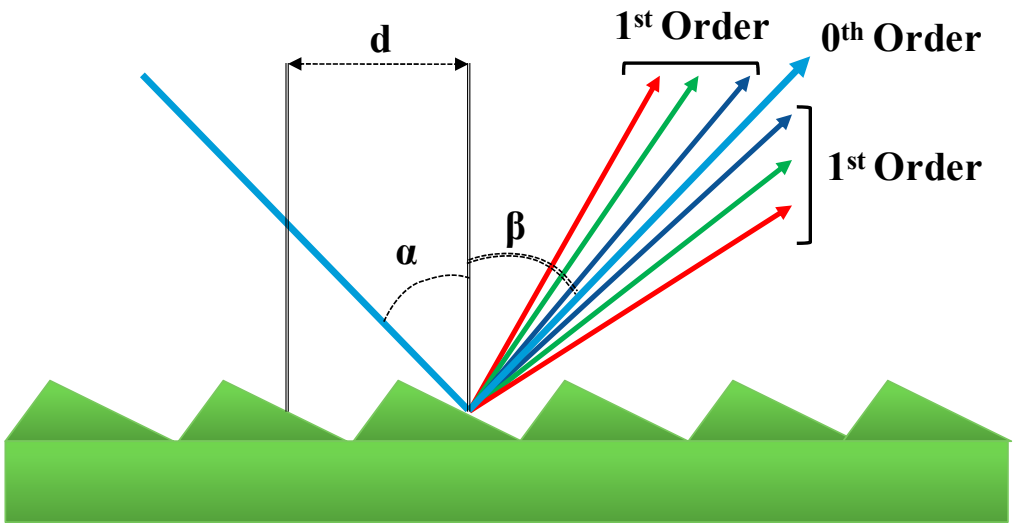

Figure 2.3. Schematic cross section of a ruled diffraction grating.

Fixed-grating spectrometers are often aligned at what is called the "blaze angle", such that collection of light from a specific wavelength range is optimized. This is accomplished by varying the parameters of the grating equation. For example, in order to optimize the collection of light at 600 nm one might use the following conditions: groove density of 1200 grooves/mm (833 nm between grooves), an angle of incidence of 45.6° and a collection angle of 11.2°. The 600 nm light collected under these conditions has a diffraction order m=1; however, the 2nd and 3rd diffraction orders also provide light at this

incidence/dispersion angle at 300 nm and 200 nm, respectively. This can be seen in Figure 2.4. To correct this issue, spectrometer manufacturers will often add wavelength-dependent filters to remove higher order (lower wavelength) light.

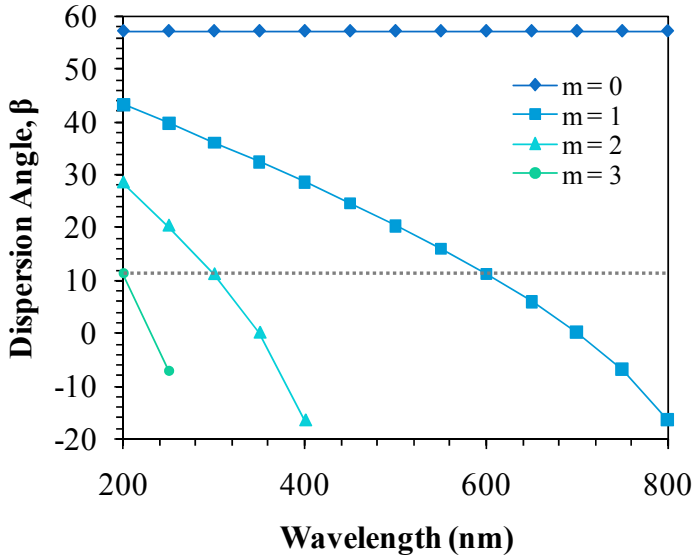

Figure 2.4. Dispersion angle as a function of wavelength for diffraction orders m=0 to m=3. The diffraction grating has 1200 grooves/mm and the angle of incidence α=45.6°.

One very common spectrometer configuration is known as Czerny-Turner (CT), shown in Figure 2.5 (A) below. Included in this setup are (1) an entrance slit, (2) a collimating mirror, (3) the diffraction grating, (4) a focusing mirror and (5) an exit slit. This instrument functions by mechanically rotating the diffraction grating, thereby varying α and β such that the output wavelength is also varied. The use of motors to vary the signal wavelength can add a considerable amount of time to the data collection process.

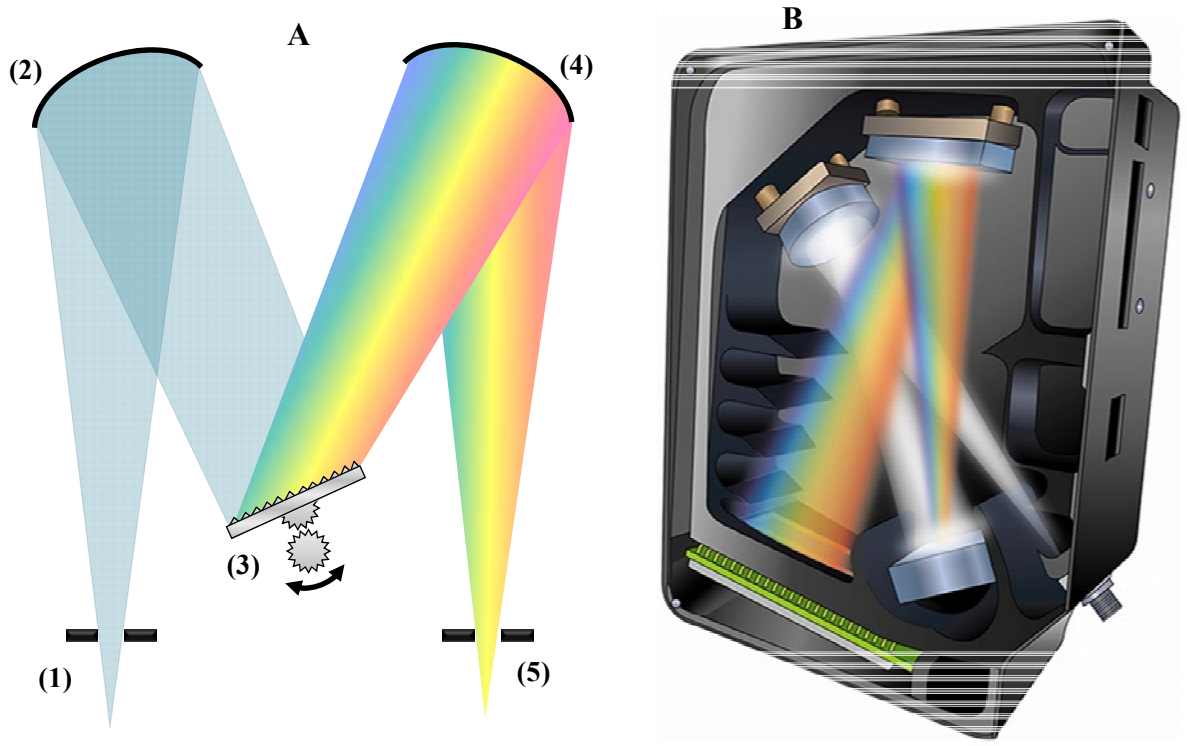

Figure 2.5. (A) Schematic of a CT spectrometer; (1) entrance slit, (2) collimating mirror, (3) diffraction grating, (4) focusing mirror, and (5) exit slit. (B) Schematic of a modified CT spectrometer. This is a crossed-beam configuration with a CCD detector rather than an exit slit.

An alternative to the rotating grating system can be seen in Figure 2.5 (B). In this setup the grating is fixed at some angle (the "blaze angle") and a CCD detector is used in place of an exit slit. The detector in this case is composed of thousands of picture elements (pixels) and is capable of measuring a broad spectrum of light. This is in contrast to the configuration with an exit slit, where a photomultiplier tube (PMT) is used to collect the light as it exits the spectrometer. The total signal bandwidth from such an instrument is on the

order of 0.01-10 nm, as compared to 100-1200 nm for a CCD-based spectrometer. Larger bandwidth is also coupled with smaller integration times, since the process of signal collection and processing lasts on the order of milliseconds rather than minutes for the scanning spectrometer. However, because of the speed with which the signal is collected and because of the physics associated with each, CCD detectors have limited sensitivity compared to a PMT. This can cause an issue with the signal-to-noise ratio for low intensity radiation. Furthermore, since CCD's are an arrangement of pixels, the spectral signal incident on one pixel is averaged across its bandwidth; hence the input signal is discretized and convoluted with a function characteristic of the detector being used.

2.3 Optical Spectra as a Convolution

It is important to recognize that the output signal of a spectrometer is not a direct representation of the light source [14]. This would only be the case for a perfect optical instrument, which for all practical purposes does not exist. There are many factors which modify the basic spectrum emitted from some source; as a matter of fact, all optical elements used in spectroscopy can alter the spectrum. In order to truly understand the nature of a spectrum (and the source of a spectrum), it is extremely important to take into account the effect a spectrometer has on a measurement.

The most common effect an instrument has on a spectrum can be seen with an ideally monochromatic light (e.g. a laser line), where all photons emanating from the source are exclusively of a single wavelength λ_o. A perfect spectrometer would measure this as a

perfectly straight line, where the photon counts I for all λ are zero, except at λ_o where $I = I_{source}$. This spectrum would be described by a Dirac delta function, which can be expressed in terms of the limit of a Gaussian distribution

$$\delta(\lambda) = \lim_{a \to 0} \frac{1}{a\sqrt{\pi}} e^{-\lambda^2 / a^2} \tag{2.1}$$

Deviations from this ideal situation arise in the form of some width a to the line. This can be seen in Figure 2.6 below. When imperfect instruments are used to measure light from a monochromatic source, one or more factors prevent the spectral output from appearing as a delta function. This is commonly referred to as "line broadening"; that is, an apparent width is added to an ideally straight line. Depending on the conditions of the plasma, an inherent width can be added to the signal which is independent of the spectrometer. A detailed discussion of this topic can be found in [15].

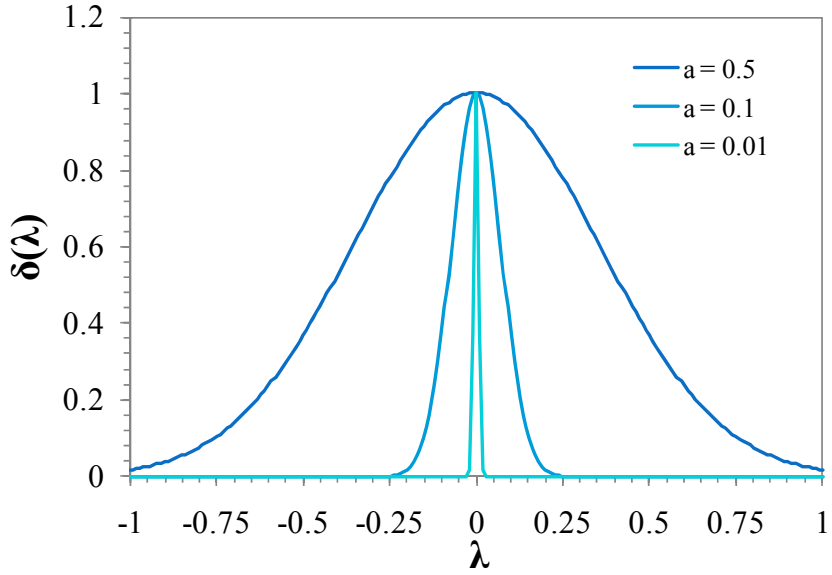

Figure 2.6. A plot of the Dirac delta function as a→0 for a Gaussian distribution.

If a spectrum is considered a continuous function, the following definition can be established

$$i(\lambda) = \int_{-\infty}^{\infty} s(\lambda - \lambda')o(\lambda')\, d\lambda' \tag{2.2}$$

where $o(\lambda)$ is the object function, or the unmodified spectrum of interest. The object function can take any mathematical form or distribution: a delta function, Gaussian distribution, Lorentzian distribution, or Voigt profile, for example. This function is convoluted with a spread function $s(\lambda)$, which inherently includes any noise or spectral broadening features. In this form, $o(\lambda)$ exists independent of $s(\lambda)$; therefore the true spectral features inherent in $i(\lambda)$ can be seen once s is extracted.

As mentioned earlier, the spread function results from a number of factors. Rather than go through each possible contribution, only the most prominent will be discussed here. For a more complete list and description of each, see [11, 12, 14, 16].

The first factor to consider is the resolving power of the spectrometer. The limit of resolution is defined as the difference in wavelength $\Delta\lambda$ required to successfully identify two adjacent peaks in a spectrum. Two peaks are considered "resolved" when the maximum of one peak falls on the minimum of the second. This is commonly known as the Rayleigh criterion. Using this guideline, the two peaks on the left in Figure 2.7 are resolved ($\Delta\lambda = \Delta\lambda_{Rayleigh}$), while the two peaks on the right are not adequately separated ($\Delta\lambda < \Delta\lambda_{Rayleigh}$) and thus are not resolved.

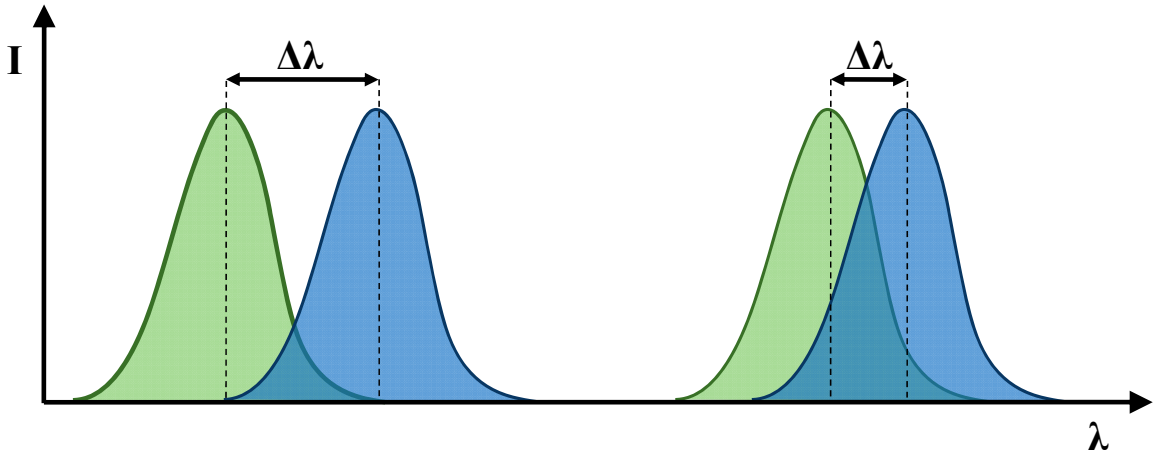

Figure 2.7. Demonstration of the Rayleigh criterion. The peaks on the left are considered adequately resolved, while the Δλ for the peaks on the right lies beyond the resolving power of the instrument.

Resolution in a spectrometer is determined by the slit width, groove density of the grating, and pixel resolution of the detector (wavelength range for an individual pixel). This theoretical resolving power is often not seen in real instruments, however, since optical aberrations convolute the spectrum with some contribution to the spread function. Moreover, in practice, the "true" spectral width of emission profiles from non-thermal plasmas [17] is often much less than the spread function of the spectrometer. This is not strictly the case for all spectrometers—astrophysical instruments often have a real resolution approaching tens of picometers—but generally true for all-purpose benchtop spectrometers. Fortunately, individual contributions to the instrumental broadening function can often be approximated as Gaussian distributions. The overall spread function can therefore be treated as a sum of squares

$$\Delta\lambda_{instrument}^2 = \sum_{i=1}^{n} \Delta\lambda_i^2 \tag{2.3}$$

where i represents each component of the instrumental linewidth. There are numerable factors which can be important, including the slit function, optical aberrations, diffraction effects or any change caused by the detector and related electrical components. Since $\Delta\lambda_{instrument}$ depends only on the spectrometer, not any particular measurement, it can be taken into account by some method of deconvolution. There is a huge volume of research based on methods for deconvolution, many of which are introduced in [16]. Once the spread function is understood and accounted for it can theoretically be extracted from any measured

spectrum. Such a process would leave only the object function—the spectrum of interest—which can then be used to determine important plasma parameters.

At this point a couple of things should be noted about this method. First, deconvolution processes are purely mathematical; that is, a deconvoluted spectrum may be mathematically correct based on the operation used but at the same time not have any physical meaning. In order to ensure that the so derived object function is indeed just that—not some contrived set of numbers masquerading as real data—one must be intimately familiar with the instrumental spread function. Considering the ease with which meaningless data is generated, it is just as easy to avoid such mistakes. When measuring well characterized light sources, such as a NIST-calibrated broadband source or monochromatic emission from a laser, the measured spectrum becomes the convolution of a known source and an unknown instrumental broadening function. In this way, the true spread function can be understood and taken into account when studying a "real" system. The other important point about this method is the more *a priori* knowledge available for a system, the better. In other words, an ideal deconvolution happens when all details of both the spread function and the object function are known. This is not a very likely (or even useful) situation, since the purpose of deconvolution is to extract information from the measured spectrum in order to learn more about the system being studied. That said, knowing more parameters initially dramatically increases the accuracy with which unknown parameters are given.

Another method commonly utilized when studying plasmas is to develop model spectra for the system of interest. By integrating fundamental relationships (power balances, force equations, state populations, etc.) with boundary conditions and system constraints (pressure, gas composition, ionization fraction, etc.), one can develop a very accurate prediction of plasma spectra. In contrast to deconvolution, which gives only indirect insight into plasma characteristics, spectral modeling is *based* on these characteristics. Artificial spectra are often built to constrain all variables except the parameter(s) of interest—electron temperature, electron temperature, or gas temperature, for example. Once the theoretical spectrum is created, it is convoluted with the appropriate spread function. This results in a model which can accurately depict measured spectral data, often to within 1% error [18]. However, developing such a model requires levels of completeness and depth which are often difficult to obtain. Open source models and fundamental experimental data are often available instead [19-21].

Overall, to generate synthetic spectra or interpret spectra derived from deconvolution, it is important to understand the relationship between light emitted from a plasma and the physical state of the emitters themselves.

2.4 Origin of Light Emission from Plasmas

One of the most fundamental features of a plasma is its propensity for releasing or absorbing electromagnetic radiation. This has led researchers to develop a staggering body of work in this area. Photon emission is extremely important for a number of reasons: it can

be a direct representation of the state of the species in the plasma; it can be amplified as a means of developing a wavelength-specific light source; and it can also represent significant energy losses in high temperature plasmas. Photon *absorption* is also very important and will be covered in section 2.5.

As a means of conserving energy, light is emitted by species which go through certain de-excitation processes. As we learned from Planck, this light is quantized; that is, the energy of each emitted photon is equal to the difference in energy between the upper and lower states of the transition. This is represented as $\Delta E = \frac{hc}{\lambda} = E_{upper} - E_{lower}$, which shows that large differences in energy between two states generate shorter wavelength light and vice versa. The quantization of light became an important topic in physics in the early to mid-20th century and actually provides the basis for spectroscopic analysis. The origin of this idea lies within quantum mechanics. According to this theory, matter—whether it's an electron, atom, minivan, or supernova—can only exist at discrete levels of energy. This is in contrast to classical theory, which allowed for matter to exist at any value in a continuum of energy.

For atoms and molecules, there exist different *types* of energy levels which can be occupied; this is controlled by what is called degrees of freedom (DOF). Let us examine a neutral helium atom as an example. Assume at first that the atom is at rest, that it can be approximated as a sphere and that an arbitrary coordinate system has been established

(Figure 2.8). If the atom now rotates, or spins, in any direction, there is no physical way to distinguish the atom's current state from its initial state—after all, it is a sphere and the coordinate system was arbitrary in the first place. Thus, the helium atom has no rotational DOF. Additionally, since helium is monatomic and has no bond along which vibration can occur, it also has no vibrational DOF. What helium does have is translational DOF, where the physical position relative to some origin can be distinct and exclusive. Helium also has distinct electron orbitals, and therefore electronic DOF (this is true for every atom and molecule). This proclivity for electronic excitation and de-excitation allows helium to emit light based on the ΔE between two electronic states.

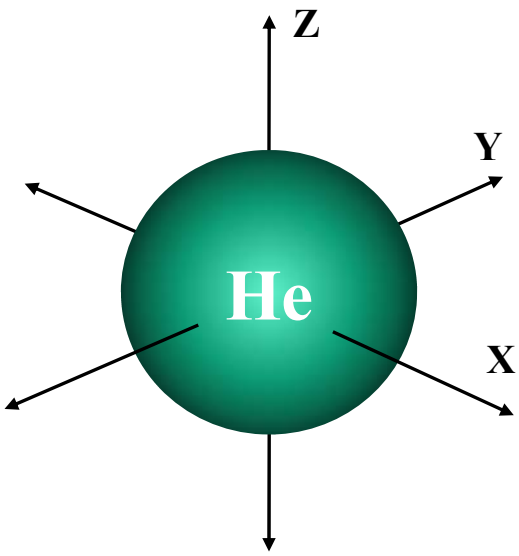

Figure 2.8. Hard-sphere schematic of a He atom with arbitrary Cartesian coordinate system.

In contrast, the OH molecule (Figure 2.9) has a permanent dipole—hence rotational DOF—and is a diatomic molecule—hence vibrational DOF. Of course it also has electronic DOF. The importance of OH and its various transitions will be discussed later.

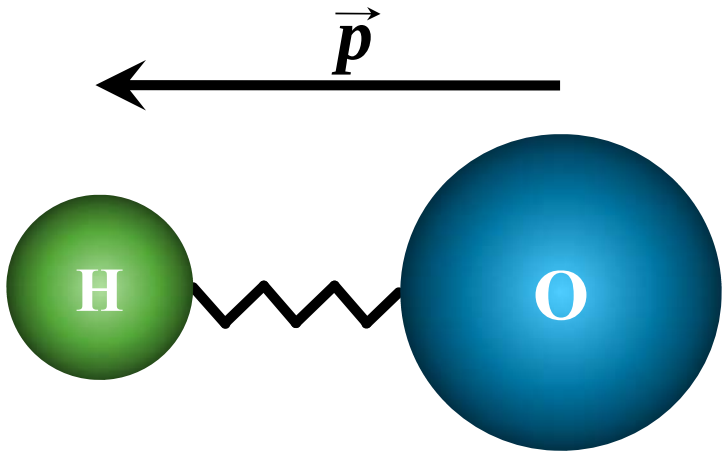

Figure 2.9. Schematic of an OH molecule, with dipole moment vector $\vec{p}$.

To summarize, energy states only exist for species with physical configurations or orientations which can be distinguished: rotational levels exist as a result of rotating electric dipoles; vibrational levels exist due to changes in the physical location of one atom relative to another atom along the length of a bond; electronic levels exist because of distinguishable orbitals which an electron can occupy. For this work, the most important types of transitions are electronic (n), vibrational (v) and rotational (J). Figure 2.10 shows an energy diagram representing these three types of levels and their relative energies.

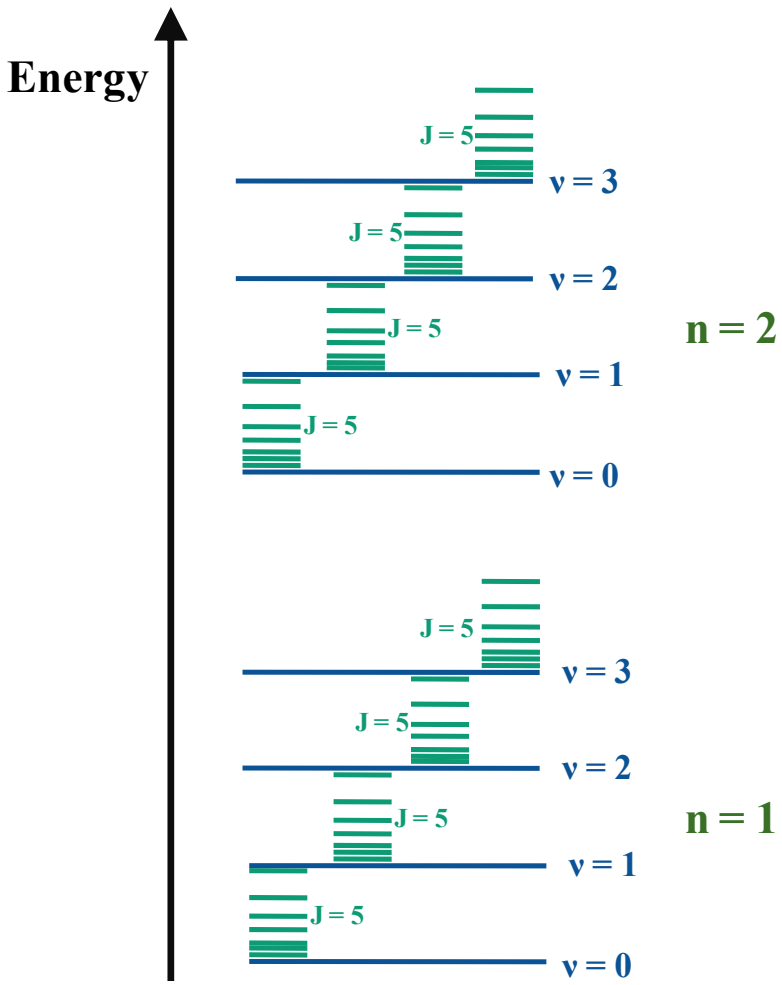

Figure 2.10. Schematic energy diagram showing the relative energies of electronic (n), vibrational (v) and rotational (J) levels.

As seen in Figure 2.10, electronic transitions represent the largest ΔE, followed by vibrational and rotational. Assuming a hydrogen-like atom, electronic energy levels can be calculated as

$$E_n = -\frac{2\pi^2 \mu e^4}{h^2}\frac{Z^2}{n^2} \tag{2.4}$$

where μ is the reduced mass of the electron and atom, e is the elementary charge of an electron, Z is the atomic mass, h is Planck's constant and n is the principle quantum number (n = 1, 2, 3, …). Electronic transitions fall in the range of 10^0-10^1 eV, or roughly the ultraviolet-visible range of light. Nearly all of the light emitted from a laboratory plasma is associated with electronic transitions, which is a result of the fact that plasmas are sustained (for the most part) by electron energetics.

Vibrational levels are given as

$$E_\upsilon = hc\omega_e\left[\left(\nu+\frac{1}{2}\right)-x_e\left(\nu+\frac{1}{2}\right)^2+y_e\left(\nu+\frac{1}{2}\right)^3+\ldots\right] \tag{2.5}$$

where ν is an integer representing the vibrational level (ν = 0, 1, 2, …), and ω_e, x_e and y_e are constants which are molecule-dependent. Pure vibrational transitions fall in the range of 10^{-2}-10^0 eV, which is the infrared range of light. These are important for infrared spectroscopy, where absorption of specific IR wavelengths corresponds to very specific bond types (i.e. carbonyl groups, C=O, absorb at 0.216-0.228 eV).

Rotational levels are given as

$$E_r = \frac{J(J+1)\hbar^2}{2\mu r_o^2} \tag{2.6}$$

where $\hbar$ is the reduced Planck's constant ($\hbar = h/2\pi$), μ is the reduced mass of the atom-atom pair, r_o is the average bond length of the transition, and J is an integer representing the rotational level (J = 0, 1, 2, …). Rotational transitions are on the order of 10^{-3} eV, or what is

commonly referred to as the microwave region of light. This point actually provides the basic operating principle for microwave ovens. The microwaves interact with water molecules in food to generate high rotational temperatures without significantly heating the oven itself. This is an efficient process due to the high levels of asymmetric heating associated with microwave radiation.

An interesting feature about plasma spectroscopy is that while electronic transitions occupy the UV-Vis range, rotational and vibrational spectra often become superimposed onto these transitions to create *rovibronic* spectra (Note: this is contrast to *rovibrational* spectra, which involves coupling between only vibrational and rotational transitions). This can be understood from Figure 2.10. Since rotational, vibrational and electronic transitions are physically independent from one another and an energy hierarchy exists between the three, lower energy transitions can be superimposed onto higher energy transitions. That is, an electronic transition may be centered near 3.17 eV / 391 nm (as is the case for N_2^+, a common feature of low temperature atmospheric pressure air plasmas), but some molecules making the transition may have more or less *rotational* energy. This affects the total energy of the molecule and hence the energy of the emitted photon; and, since rotational transitions are quantized—just like electronic and vibrational transitions—this arises as a series of emission lines closely spaced around a strong emission line (also known as the band head). As an example of this phenomenon, emission spectra of N_2^+ at 500 K were simulated at different instrumental resolutions using the LIFBASE software (Figure 2.11).

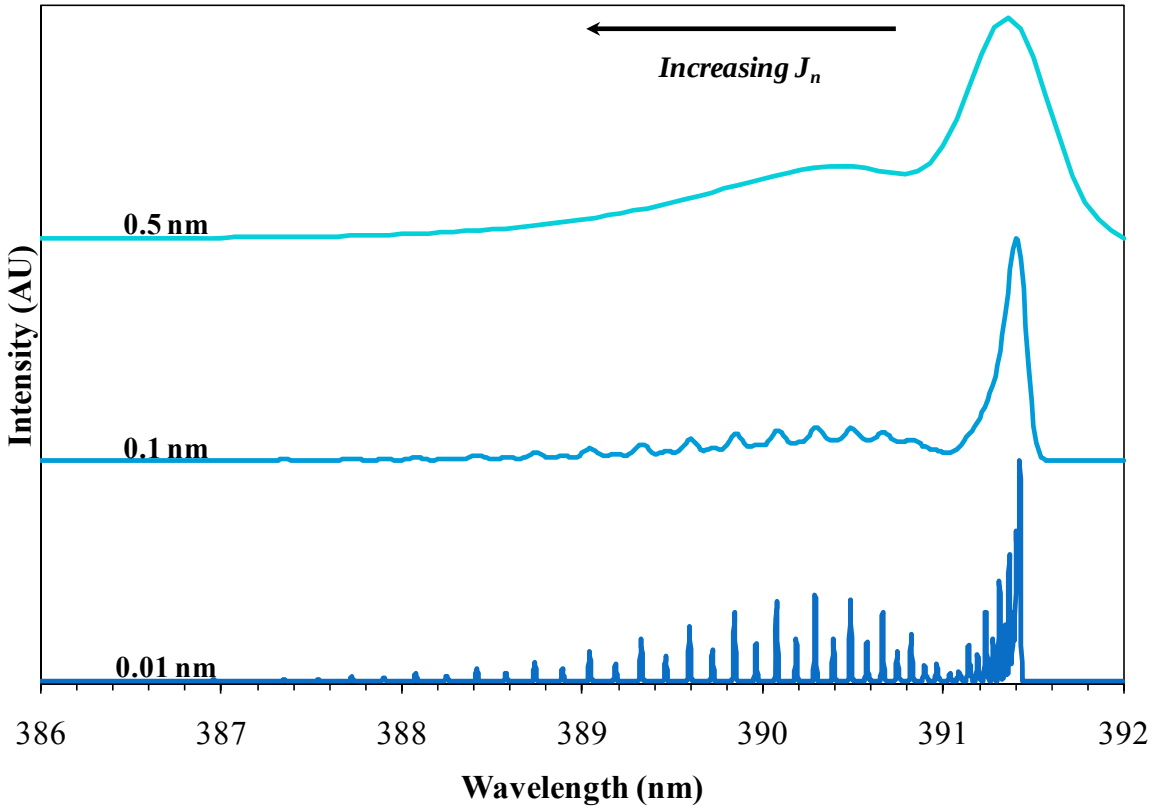

Figure 2.11. Simulated spectra of N_2^+ ($B^2\Sigma_u^+$, v=0 → $X^2\Sigma_g^+$, v'=0) at 500 K, with instrumental resolutions of 0.01 nm, 0.1 nm, and 0.5 nm.

As one might expect, the intensity of emission lines from a plasma can be related to the number of molecules in a particular state. This is strictly true only for (a) transitions involving the ground state and (b) environments controlled solely by electronic collisions (i.e. no interactions with metastables, bond dissociation reactions or any other secondary de-excitation process) [22].

To a first order approximation, the distribution of molecules in rotation and vibrational energy levels is controlled by the temperature of the molecules themselves. While most

laboratory plasmas are not controlled by thermal processes—that is, they are controlled by electron excitation—the partition functions still follow a thermal distribution. This results from the fact that the small electron mass does not significantly change a molecule's angular momentum upon collision. For vibrational states, the populations N_v are governed by

$$N_v = e^{-E_v/kT} \tag{2.7}$$

where E_v is equation (2.5), and T is the temperature. Since vibrational transitions require 10^{-1}-10^{0} eV, the thermal energy from plasmas is often not enough to promote excitation above *v=0* or *v=1*. This can be seen in Figure 2.12, which shows the vibrational population of OH for different temperatures. It should be noted here that the actual population distributions are not continuous, as Figure 2.12 seems to imply. Instead, molecules may *only* occupy the specific vibrational levels (*v = 0, 1, 2*…) and no value in between. The same is true for rotational population distributions seen in Figure 2.13.

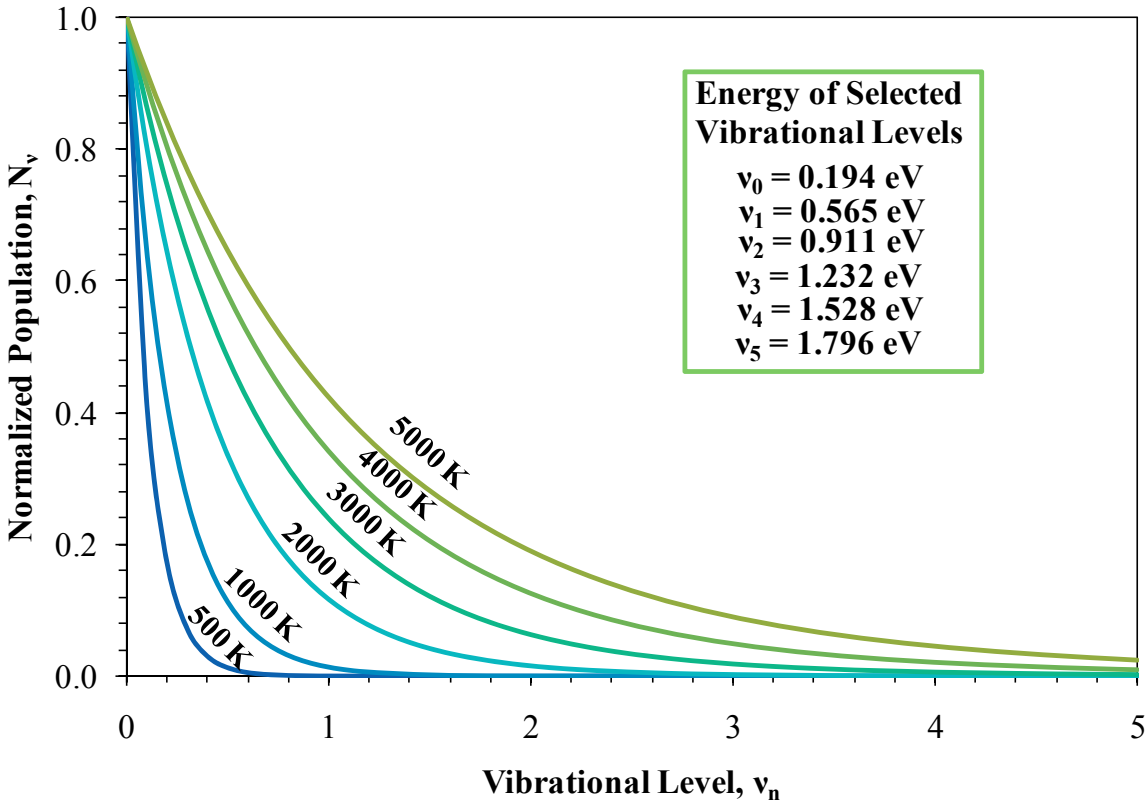

Figure 2.12. Population of vibrational levels at different kinetic temperatures for OH. As a means of comparison, energy values are given for specific vibrational levels.

In contrast to vibrational transitions, rotational transitions require much less energy; therefore, rotational partition functions are much more sensitive to changes in temperature. The number density of molecules at a particular rotational level is given by

$$N_J = (2J+1)e^{-BJ(J+1)hc/kT} \tag{2.8}$$

where B is the vibrational constant, J is the rotational level and T is the temperature. The temperature-dependent distributions of the OH molecule can be seen in Figure 2.13.

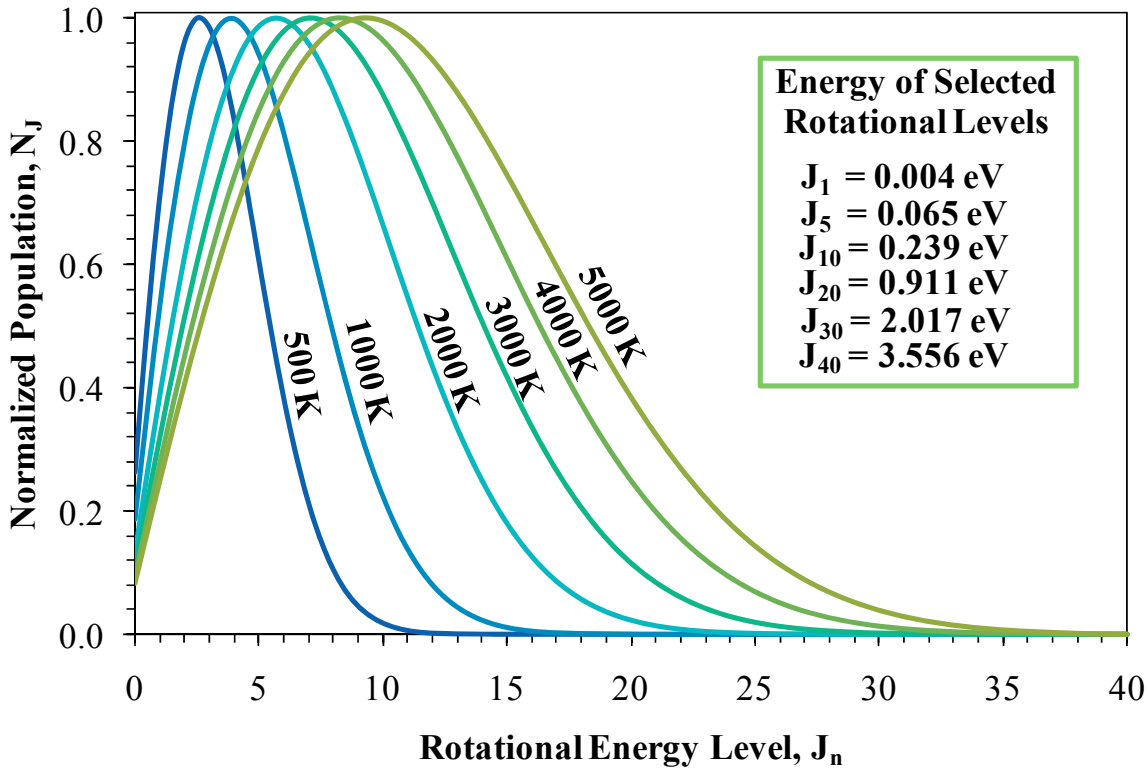

Figure 2.13. Distribution of OH molecules in rotational levels J_n for various temperatures. As a means of comparison, energy values are given for specific rotational levels.

By taking both rotational and vibrational population distributions into account, and keeping with prior assumptions, the intensity of an emission line is given as

$$I = \frac{C_{em} v^4}{Q_r}\left(J' + J'' + 1\right) e^{-B'J'\left(J'+1\right)hc/kT} \tag{2.9}$$

where v is the vibrational level, Q_r is the rotational state sum, J' is the upper rotational state, J'' is the lower rotational state, B' is the modified vibrational constant, T is the temperature, and C_{em} is a constant which depends on the dipole moment change and the total

number of molecules in the initial vibrational level. By using a program called LIFBASE [19], the theoretical spectrum for OH at different temperatures can be found (Figure 2.14).

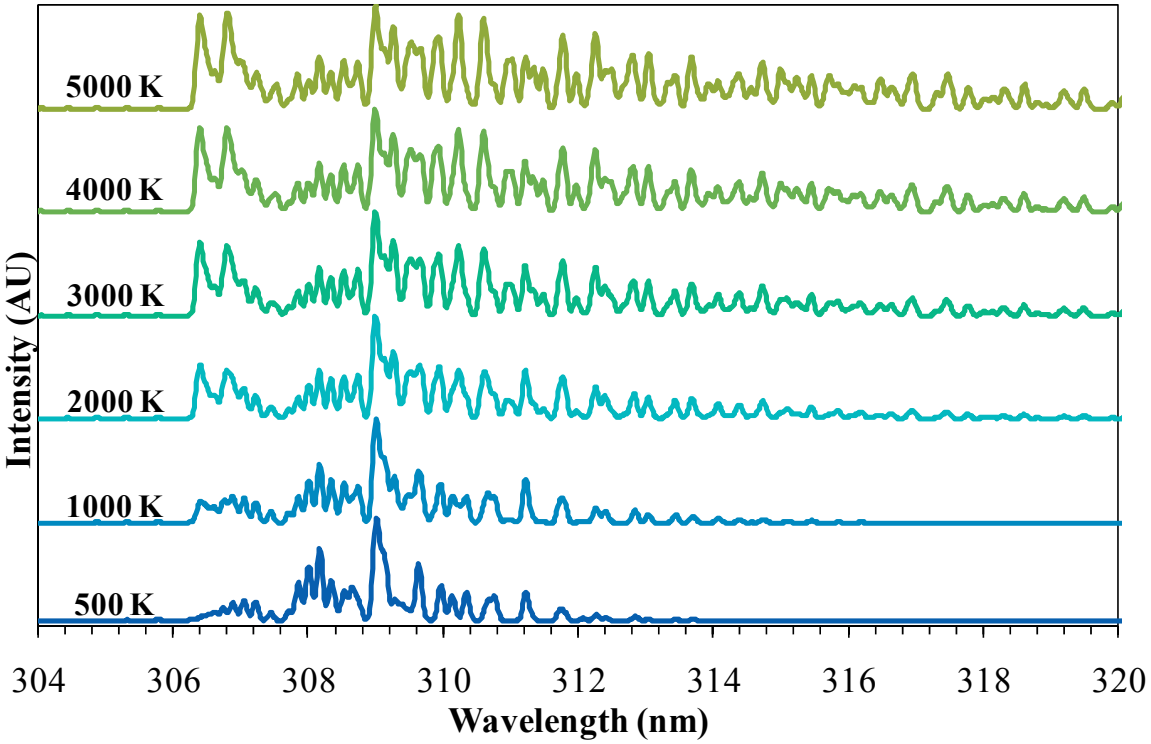

Figure 2.14. Theoretical emission bands of the OH molecule at various temperatures.

The temperature dependence of emission bands leads to another important topic in plasma spectroscopy: determination of temperatures within a plasma. This is often a difficult task, as most conventional methods require a probe of some kind (e.g. a thermocouple) to be inserted into the plasma, which creates perturbations and is often impossible due to material limitations (i.e. probe melting). Noninvasive methods were developed to overcome this problem, one of which is optical spectroscopy. A large body of

work exists on this topic, and researchers routinely measure temperatures to within a couple of percent [23]. The plasma temperature measurements in this work also utilize emission spectroscopy. Since rotational level populations are much more sensitive to changes in temperature than vibrational populations, the "rotational temperature" can be taken as an estimation of the actual gas temperature inside the plasma.

2.5 Light Absorption in Plasmas

In way photons of specific energies can be *emitted* by atoms and molecules, photons can be *absorbed* with similar specificity. This is true for both active species within the plasma and stable states outside the plasma. Absorbance A is a wavelength-dependent and concentration dependent phenomena, given by the Beer-Lambert law

$$A = \ln\left(\frac{I}{I_0}\right) = \sigma_{abs} N l \tag{2.10}$$

where I_0 is the initial intensity of a light beam, I is the final intensity after passing through the absorption path length l, σ_{abs} is the absorbance cross section for a given wavelength, and N is the number density of absorbers.

Since species at a given energy level respond to specific photon energies, and since this absorption is concentration-dependent, absorption spectroscopy is an extremely useful tool for real-time process analysis [24]. Broadband sources can often be used for stable molecules found outside the plasma; however, for excited species within the plasma a monochromatic light source must be used.

2.6 Summary

The preceding sections provide the basics for optical analysis of plasmas. These ideas will be used for analysis of the plasma studied in this work. For a more in-depth treatment of various optical analyses, or for other application-specific techniques, see [15, 17, 22, 25, 26].

3 Experimental Summary

3.1 Reaction Chamber

3.1.1 Reactor Design

The reaction environment for these experiments consisted of a cylindrical quartz chamber 10.13 cm in diameter and 30.5 cm long, or a volume of about 2.5 liters. The top and bottom flange of the reactor were stainless steel and Delrin, respectively. Hollow, cylindrical, stainless steel electrodes were used in this study, 0.635 cm diameter x 6.5cm long. They were arranged vertically and slightly sub-parallel to one another, with a gap distance of 2.54 cm. The experimental setup can be seen in Figure 3.1.

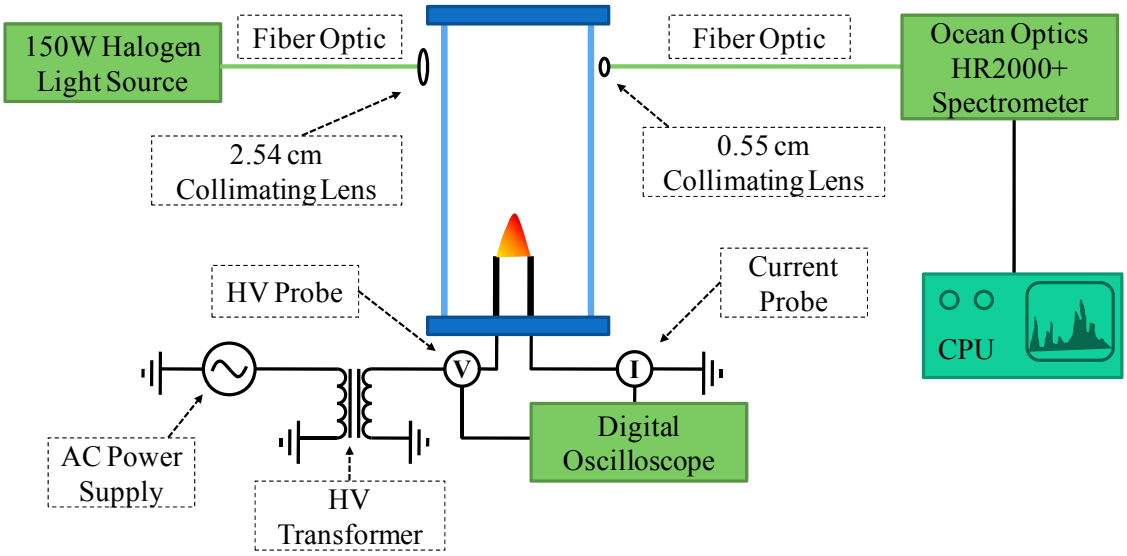

Figure 3.1. Schematic of the experimental setup.

3.1.2 Gas Delivery

Ultra high purity nitrogen (99.999%) and ultra high purity oxygen (99.999%) were used in varying ratios (4N:1O, 1N:1O and 1N:4O) for these experiments, controlled by mass flow controllers. Before each experiment the chamber was evacuated to 10^{-1} Torr using a rotary vane mechanical pump and filled to atmospheric pressure using the appropriate gas mixture. Pressure was monitored using a convectron gauge.

3.1.3 Power

The discharge studied in this work was an AC-driven arc at atmospheric pressure. The discharge was generated and sustained using a commercial power supply (AIR-DBD-5000, AP Solutions Inc, Cary NC). This source was connected to a high voltage transformer with three principle coupling harmonics. In this way the discharge could be both frequency modulated and power modulated. The electrical measurements were taken using a Tektronix P6015A high voltage probe and a Pearson Electronics Model 4100 current monitor. Data from these probes were collected with a Tektronix TDS-5034 digital phosphor oscilloscope, 350 MHz bandwidth.

3.2 Optical Measurements

3.2.1 Spectrometers

Both absorption and emission measurements were carried out with an Ocean Optics LIBS2000+ setup. This is a 7-channel spectrometer arrangement capable of measurements

from 200-900 nm, with each channel corresponding to a range of about 100 nm. The groove densities for each channel are as follows:

Table 3.1 Ocean Optics LIBS 2000+ Spectrometer information.

Channel #	Wavelength Range	Grating Groove Density
1	200-300 nm	2400 lines/mm
2	300-400 nm	2400 lines/mm
3	400-500 nm	1800 lines/mm
4	500-600 nm	1800 lines/mm
5	600-700 nm	1800 lines/mm
6	700-800 nm	1800 lines/mm
7	800-900 nm	1200 lines/mm

The detector for each channel is a 2048 pixel linear CCD array. Light emitted from the plasma and reference light source (when used) were collected using an optical fiber and a 0.55 cm collimating lens. The halogen lamp was also coupled to an optical fiber and a 2.54 cm collimating lens.

3.2.2 Absorption Measurements

Absorbance measurements were used to determine the NO_2 density as a function of time in the reactor, found via the Beer-Lambert law (Equation 2.10). Light emission in the visible range, produced from a 150 W broadband halogen lamp, was used as the reference light source. This lamp was chosen as the appropriate reference for two reasons. Photon energies of 3.118 eV and above (corresponding to $\lambda \leq 398$ nm) are at the photodissociation limit for NO_2 [27]; hence UV lamps conventionally used for absorbance measurements of nitrogen oxides would actually have an impact on the gas chemistry of interest. The second reason is that NO_2 is the only potential absorber with an appreciable cross section in the visible range.

This greatly simplifies data collection and analysis, as more species would otherwise need to be taken into account.

In reference [28] a high resolution absorbance cross section for NO_2 in most of the visible range was provided by generating a temperature dependent analytical function for the absorption envelope. The cross section shows a weak temperature dependence from 400-500 nm, so observed temperature gradients along the light path can be ignored. The line averaged absorbance at 470 nm was used for all calculations of NO_2 density.

Data collection for NO_2 density calculations were given by line-averaged absorption measurements taken every 5 seconds throughout the course of each experiment. Transmitted light was collected for 900 msec over the wavelength range of the detector and the final result was taken as the average of 4 data collection cycles. The NO_2 absorbance cross section essentially consists of noise (resulting from coupled rotational-electronic transitions) superimposed onto an absorbance envelope. Therefore, a moving average smoothing technique with a window width of 5 points was used to approximate the experimental data as a smooth function and decrease the noise inherent in such a measurement. The smoothing process begins at one end of the detection channel and averages four nearest-neighbors of a center point. Iterations of this process are completed by changing the center point in a step-wise fashion until reaching the final pixel of the channel.

3.2.3 Emission Measurements

Optical emission spectroscopy (OES) was used to measure photon emission from the plasma. Light signatures based on radiative deexitation of active species in the plasma provide a means of establishing the presence of important chemical radicals in the plasma; in particular we are interested in compounds that provide formation and destruction mechanisms for NO_2. Emission from the 0-0 vibrational band of O_2 ($b^1\Sigma_g^+ \rightarrow X^3\Sigma_g^-$, 758-772 nm) and atomic O triplet state ($^5P \rightarrow ^5S$, 777 nm) were measured for each gas ratio. These are highly reactive species and therefore provide insight into dominant reaction pathways within the plasma.

3.3 Ambient Gas Temperature Measurements

The ambient gas temperature inside the reactor is an important factor in terms of plasma chemistry. Measurements were taken for the full length of each experiment, both for the sake of using the appropriate temperature-dependent absorbance cross section and for correlating NO_2 generation to ambient gas temperature. The measurement was carried out using a type-K thermocouple, 5 cm directly above the discharge. The gas mixing ratio was 4N:1O and the applied power was 90 W. These experiments were completed with a static volume of gas—that is, no flow through the reactor—at the given mixing ratio.

4 Nitrogen Dioxide Synthesis

4.1 Introduction

The chemistry evolved from air plasmas is of great interest, from both a pure science and application standpoint. Highly active radicals such as O, O_3, OH, and various nitrogen oxides (NO_x) are often produced in great quantities, along with significant UV radiation. Individually or combined, these products have been utilized in a large number of multi-disciplinary applications. For example, applications in biomedicine and biochemistry [29-32], sterilization [33, 34], surface modification [35-39], and contaminant abatement [40-47] are currently of great interest.

In spite of their utility, factors that facilitate and control the production of active species in air plasmas are complex and interdependent [48]; hence they can be difficult to study. Also, varying parameters such as electrode configuration, operating pressure, gas temperature, electron temperature and density, and input power can produce vastly different results. It is therefore very important to understand dominant formation mechanisms for species of interest.

This work focuses on NO_2 production in an atmospheric pressure plasma. The motivations for this study are twofold. First, this particular compound is ubiquitous in all atmospheric pressure discharges containing nitrogen and oxygen [18, 49], and it is also toxic. The latter often prevents these discharges from making their way beyond a controlled laboratory environment. It is therefore important to understand the conditions which

promote NO_2 formation. Second, while NO_2 can be an unwanted byproduct of plasma processing in air, it is also a required compound for the synthesis of nitric acid and ammonium nitrate fertilizers (via the Ostwald and Haber processes, respectively). Therefore, understanding which factors control NO_2 formation could lead to a technology whose efficiency surpasses current processes.

This idea has been evaluated in the past [1]; however the process was found to be non-economical due to electricity costs. The types of discharges used in the production (or destruction) of NO_2 from air were either high temperature arcs [1, 50-53], corona discharges [54-58], dielectric barrier discharges [59-61], or low pressure glow discharges [62-67]. Each of these discharges has drawbacks for NO_2 generation: high current arcs are not energy-efficient enough to be considered economical; the operating temperature of corona discharges is too low; dielectric barrier discharges are limited in their power input; and low pressure discharges suffer from minimal throughput. Thus a discharge is needed which can overcome the numerous limitations.

This chapter details an experimental study of NO_2 synthesis using an atmospheric pressure arc in air, i.e. the plasma flame. The effects of nitrogen to oxygen ratio, plasma reaction time, radical chemistry and heat generation on NO_2 production were studied. Power and frequency were held constant in these experiments in order to develop a preliminary understanding of reaction chemistry and thermal effects. Chapter 5 on the other hand

exposes the effects of power and frequency on radical chemistry, which is then related to NO_2 generation.

4.2 Experimental

4.2.1 Discharge and Reactor Characteristics

Physical characteristics of the discharge reactor are detailed in section 3.1. For each experiment the chamber was evacuated and subsequently filled with a specific nitrogen to oxygen ratio (4N:1O, 1N:1O, 1N:4O). Once at atmospheric pressure, the gas flow valves were closed such that the overall reaction consisted of a single volume of gas. The plasma was then ignited for a certain period of time (30 sec, 1 min, 2 min, 5 min, and 10 min) and subsequently extinguished. A single frequency of 159 kHz was used for all experiments in this work, as this typically provides the most stable discharge for the conditions presented here. The voltage and current levels, measured as the RMS of each waveform, were also held constant at 1.6 kV and 60 mA, respectively.

4.2.2 Data Collection and Spectrometer Setup

Optical emission measurements were taken as the average of 10 spectra, each with a 3 second integration time, and corrected for electrical dark and ambient light. Emission from excited O_2 and atomic O were measured and correlated to NO_2 production.

Absorbance measurements were used to determine the concentration of NO_2 produced by the discharge. Spectra were taken with a moving average window width of 5 pixels, at an integration time of 900 msec and averaged over 4 cycles. Each of these spectra were

collected at 5 sec increments, starting from the point at which the plasma was turned on and ending 3 min after the plasma was turned off. This method allowed for investigation of NO_2 concentration through the entire dynamic range of its formation.

4.3 Results and Discussion

4.3.1 Electrical Properties of the Discharge

The current associated with the plasma is orders of magnitude lower than common atmospheric pressure arcs (e.g. arc welders). Such low current precludes complete thermalization and allows for production of active metastable species, as seen in non-equilibrium discharges. There is likely a spatial transition in the discharge from local thermodynamic equilibrium (LTE) to non-LTE, which is the subject of future work. However, from a preliminary standpoint, it is clear that the high temperature "core" of the plasma is responsible for generating high gas temperatures within the plasma. Reduced temperatures in the periphery of the discharge allow energy to be deposited into chemically important electronic and vibrational states, rather than being distributed into chemically useless modes.

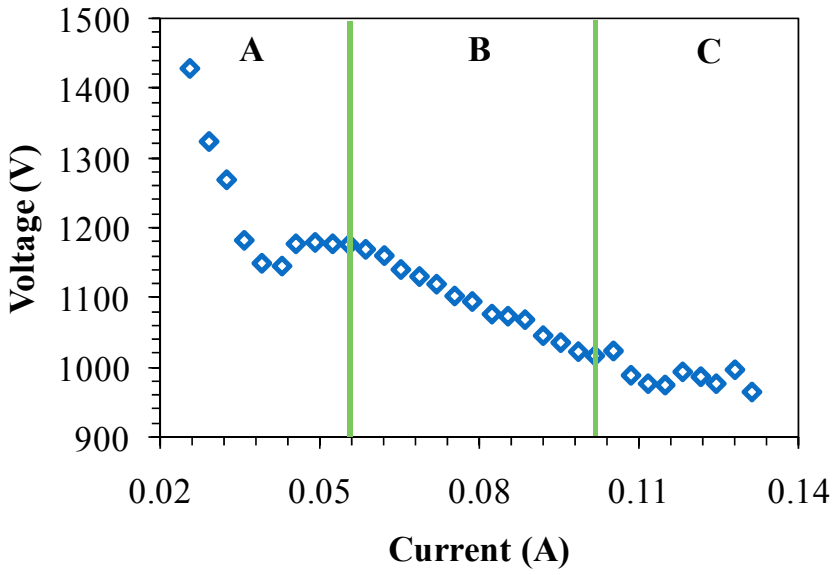

Figure 4.1. Current-voltage plot for plasma flame, where regimes A, B and C represent different discharge modes.

The current-voltage characteristics of the discharge were measured at a gas mixing ratio of 4N:1O to investigate the electrical properties of the discharge. Figure 4.1 clearly shows the negative differential resistivity which is typical of atmospheric pressure arcs [26]. Moreover, three separate IV regimes—A, B and C—can be delineated based on functional linearity. Region A represents an almost entirely non-thermal discharge, where the thermal core comprises <1% of the total discharge volume. Region B is the most stable through the IV-space covered here, and represents a higher level of thermalization. That is, the thermal core expands to 1-30% of the total discharge volume. This change most likely originates from increased thermionic emission as the electrode temperature increases. Region B is very useful for operation since the thermal core provides enough heat to the ambient gas to sustain

reactions with large activation energies, but not so much heat that it loses the excitation specificity associated with non-equilibrium discharges. Region C, on the other hand, represents significant instabilities in the discharge. Here the discharge length is constantly changing—hence the voltage is also changing—and the thermal core has fully expanded to occupy most of the total volume. This IV regime is relatively useless for the purposes of this work since (1) it is so unstable, (2) the non-thermal region is almost non-existent and (3) there is significant electrode erosion. All experiments for this work were within region B of the IV plot.

Ohm's law is satisfied in region B since a linear relationship exists between current and voltage. From this, the impedance Z can be calculated as the slope V/I, which turns out to be 3570 Ω.

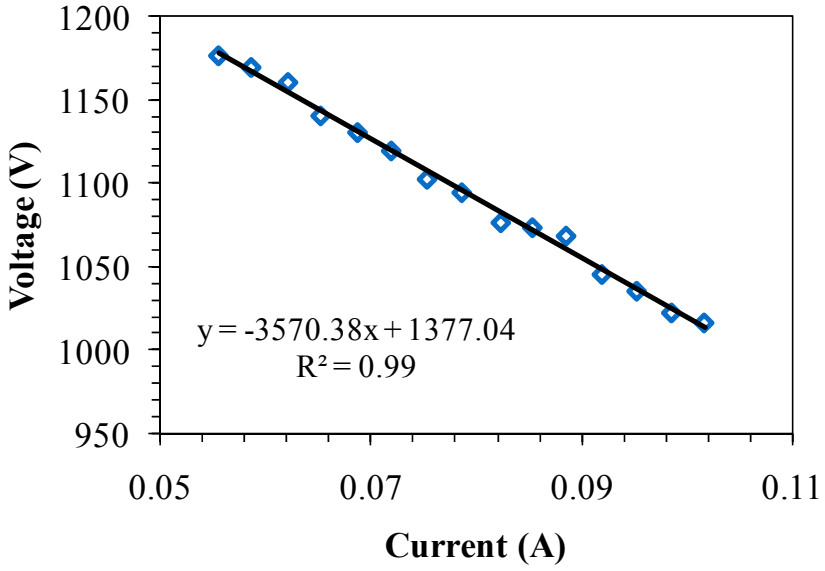

Figure 4.2. Region B of IV plot with linear trendline. The slope of the line V/I is the resistance R, which is linear throughout region B.

Impedance is defined as

$$Z = R + jX \tag{4.1}$$

where R is the resistance, $j = \sqrt{-1}$ and X is the reactance. If the reactive components are considered negligible (this assumption will be evaluated below), the impedance is composed only of resistance and

$$Z = R = \frac{l}{A}\eta \tag{4.2}$$

where l is the plasma length, A is the cross-sectional area and η is the plasma resistivity. If electrons are assumed to be the main charge carriers in this discharge,

$$\eta = \frac{m_e \nu_{en}}{n_e e^2} \tag{4.3}$$

where m_e is the electron mass, ν_{en} is the electron-neutral collision frequency, n_e is the electron number density and e is the charge of an electron. The collision frequency for air plasmas with moderate electron temperatures (1-2 eV) is tabulated in the literature [26], and is based on an effective pressure p_{eff}. This takes into account the process pressure and ratio between the temperature at STP and the gas temperature inside the plasma, $p_{eff} = pT_{STP}/T_{gas}$.

The expected plasma resistance R_p can be calculated by assuming l = 3 cm, the plasma diameter is 0.5 cm, and the electron number density is 10^{13} cm^{-3}. This calculation yields ~ 27 ohms, which is much less than the measured impedance; hence the assumption of pure resistance must be evaluated.

If an inductive component is included in the model of the plasma impedance,

$$Z = R_p + j\omega L_p \tag{4.4}$$

where ω is the driving frequency (158 kHz) and L_p is the plasma inductance, which is equal to $\nu_{en} R_p$. The magnitude of this statement gives a value for R_p which approaches 10^{-12} ohms. This also yields an incorrect model of the plasma. If a capacitive component is included in the plasma impedance,

$$\frac{1}{Z} = \frac{1}{R_p} + j\omega C_p = \frac{1 + j\omega R_p C_p}{R_p} \tag{4.5}$$

where C_p is the plasma capacitance. If the R_p is taken to be 27 ohms as calculated above, C_p ~25 nF. This capacitance is not negligible, but it is small enough to not significantly affect the discharge. Therefore, equation (4.2) will be used as the plasma model.

The electron number density can now be calculated from the following expression [68]

$$n_e = \frac{l}{RA}\frac{m\nu_{en}}{e^2} \tag{4.6}$$

Since the cross sectional area of the plasma varies through its length—i.e. the diameter is small near the electrodes and expands toward the center of the plasma—the number density should also vary through the plasma length. While not a direct measurement, calculating n_e as a function of plasma diameter gives an indication of spatial variations in number density. This can be seen in Figure 4.3.

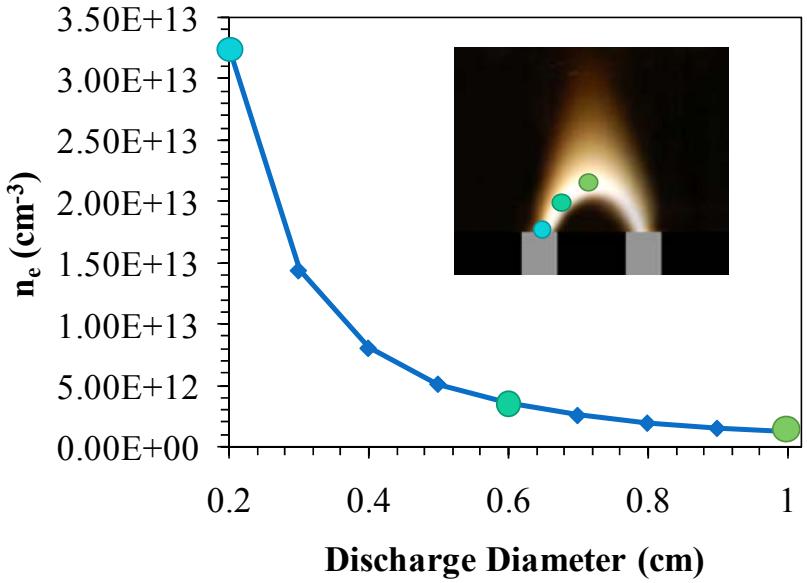

Figure 4.3. Variations in electron number density with cross-sectional area of the plasma.

Plasmas with n_e in the upper 10^{12} and lower 10^{13} are considered on the boundary between thermal and non-thermal discharges [17, 18]—that is, they are considered to be hybrid discharges [68]. This level of ionization is a defining characteristic of the plasma flame. In addition to n_e, temperature also plays an important role in the plasma flame's unique mode of operation, as will be discussed in section 4.3.4.

While in the mode of region B, the discharge remains stationary on both electrodes and is therefore stable throughout its current and voltage regime. Often, however, the discharge will jump to a new location on one or both of the electrodes, thereby increasing the voltage necessary to sustain its operation. This results from the fact that the electrodes are flat at the ends rather than terminating in a point. Strong thermionic emission is always coupled with the increase in voltage, in order for the discharge to remain self-sustained. Operation in this mode is characterized as region C in Figure 4.1 and Figure 4.4.

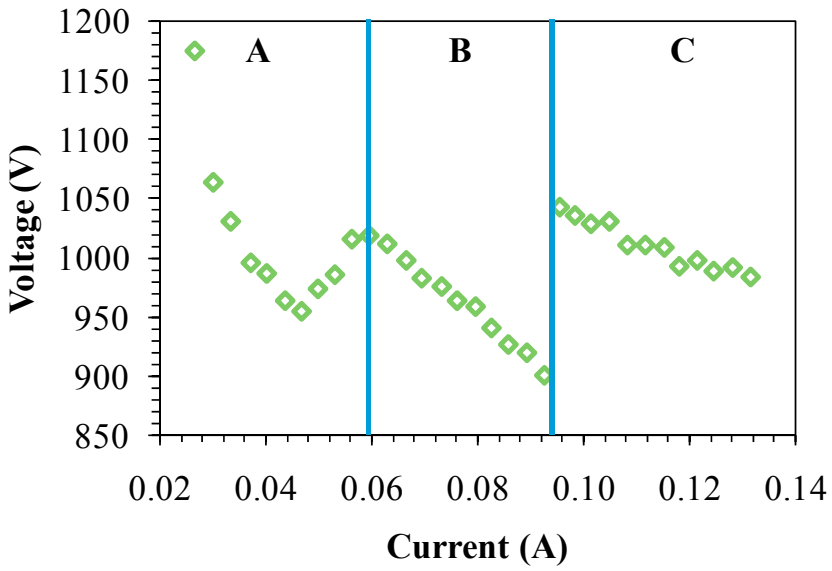

Figure 4.4. IV plot for plasma flame where regions A, B and C represent different modes of operation. This data was obtained when region C began to dominate.

Figure 4.4 shows a situation where the plasma jumped to a new location on one of the electrodes, thereby stabilizing region C throughout a larger portion of IV-space. A distinct twofold reduction in resistance is found in this region, as seen in Figure 4.5, which is a result of increased thermionic emission from the electrodes.

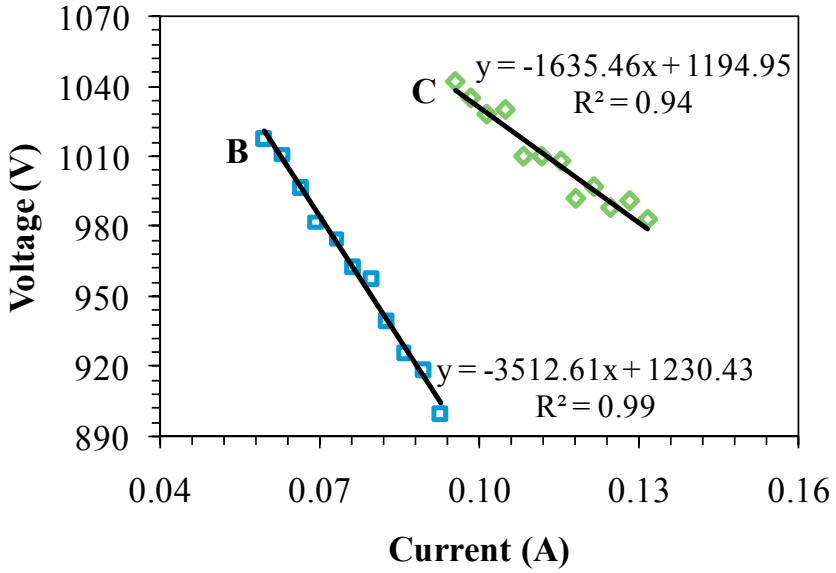

Figure 4.5. IV characteristics of regions B and C in Figure 4.4. The resistance of region C is almost half that of region B.

Furthermore, the number density of electrons in this mode increases in region C (Figure 4.6). A feedback loop exists between R, n_e and plasma temperature such that more electrons from thermionic emission increases the temperature of the plasma and decreases the resistance, thereby further increasing the current and n_e.

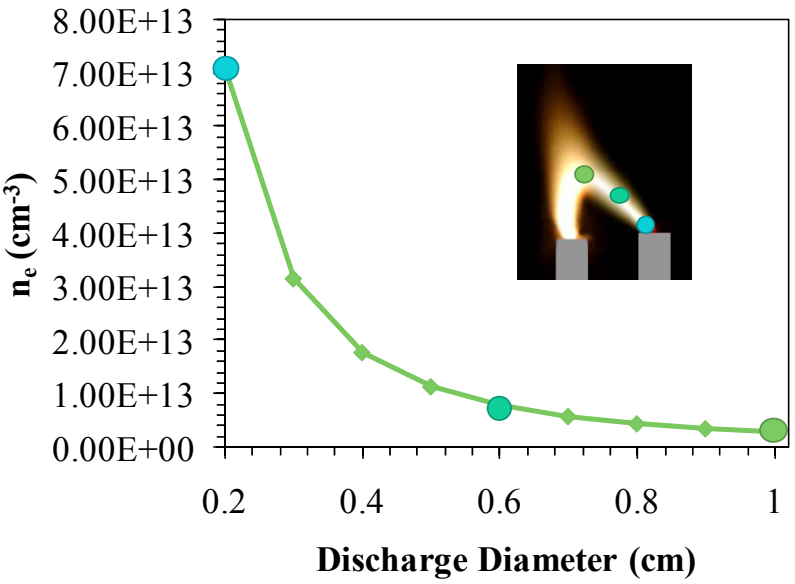

Figure 4.6. Elecron number density at various discharge diameters for region C.

As mentioned before, region C is undesirable in terms of plasma chemistry. It is therefore prudent to prevent the transition, either by cooling the electrodes or using electrodes which terminate in sharp points.

4.3.2 Radical Production

Formation of NO_2 in air plasmas is predicated on the availability of a number of different species. To a first order approximation, this includes N_2, NO, O_2, O, and O_3 [18]. For this work, the relative emission of O and O_2 were measured for each gas mixing ratio. These were the only species measured out of the list above because either (a) the other emission bands were washed out by broadband emission (NO and N_2) or (b) high temperatures prevent formation of the molecule within the plasma volume (O_3). In any case, the measured

bands represent significant chemical reactivity within the plasma and give a relative indication of important reactants for NO_2 formation.

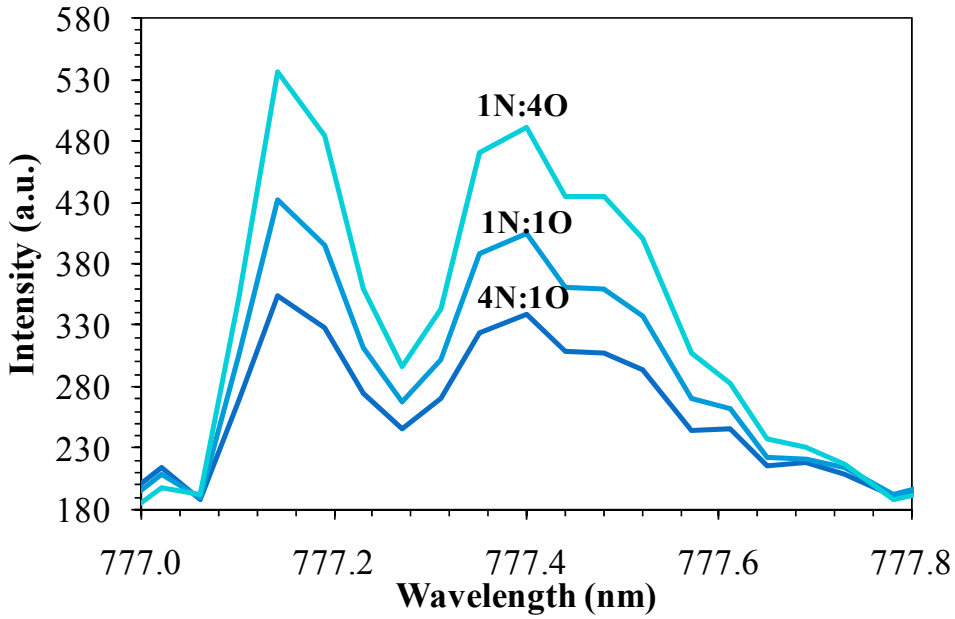

Figure 4.7. Relative emission of atomic O ($^5P \rightarrow ^5S$, 777 nm) for gas mixing ratios of 4N:1O, 1N:1O and 1N:4O.

Based on Figure 4.7, it is clear that the gas mixing ratio has a significant effect on the population of O within the plasma. In particular, the proportion of O increases with increasing oxygen content in the feed gas. This turns out to be an important point, one which will be covered in Chapter 5.

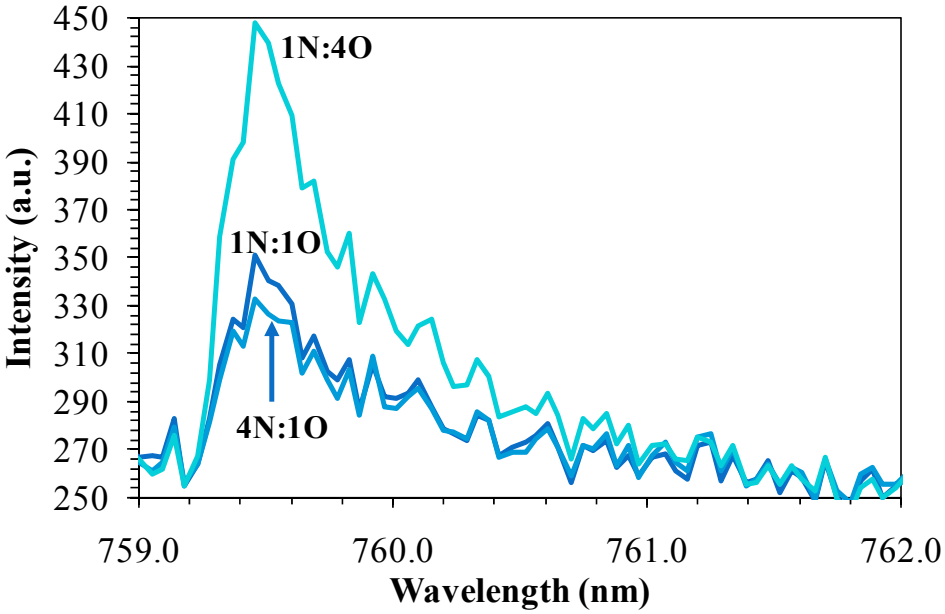

Figure 4.8. Relative emission of 0-0 vibrational band of O_2 ($b^1\Sigma_g^+ \rightarrow X^3\Sigma_g^-$, 758-772 nm) for gas mixing ratios of 4N:1O, 1N:1O and 1N:4O.

Figure 4.8 shows a similar dependence between excited O_2 emission and gas mixing ratio. This band is relatively weak in air plasmas and tends to become prominent only when oxygen is in excess [23].

With an idea of the relative population of these active species, one must look to reaction kinetics in order to determine how the species are being consumed in the plasma.

4.3.3 Reaction Kinetics

This section investigates the evolution of NO_2 as a function of time in the gas mixtures 4N:1O, 1N:1O and 1N:4O. Once the chamber was filled with a specific gas mixture, the plasma was turned on for a specific length of time (30 sec, 1 min, 2 min, 5 min or 10 min)

and then turned off for 3 min. The results from 4N:1O can be seen in Figure 4.9. It was found that for all plasma reaction times (length of time the plasma was "on") the NO_2 concentration increased at the same rate. As seen in the figure, the upper concentration limit before the plasma was extinguished was mostly determined by the total plasma reaction time. After 5 min, however, the concentration levels off and remains constant while the plasma is on. In other words NO_2 formation is rate limited until approximately 5 min, at which point it becomes volume limited.

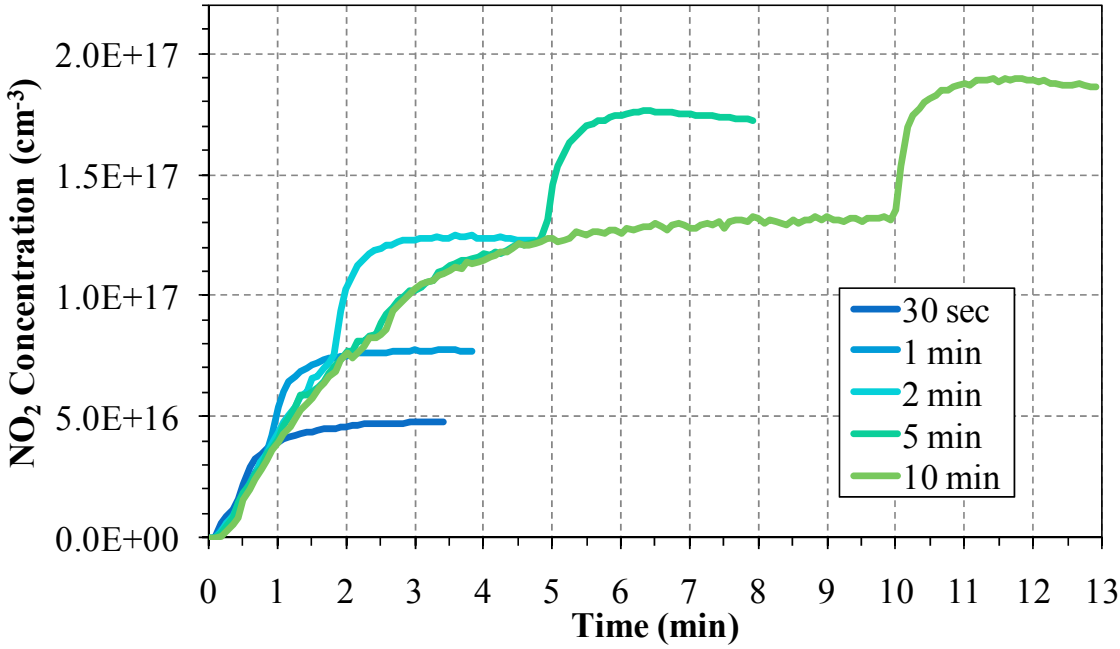

Figure 4.9. NO_2 formation in the plasma flame at a gas mixing ratio of 4N:1O.

An interesting feature is then observed once the plasma is extinguished. For all plasma reaction times, as soon as the plasma is turned off and for about 15-30 sec thereafter, the

NO_2 density increases at a high rate before leveling off again. The mechanism for this sudden increase will be discussed below.

To determine the effect of gas composition on NO_2 formation, two other variations of the gas mixing ratio were used, 1N:1O and 1N:4O. In this way the effective volume of the reactants were varied such that important reactions could be artificially starved or promoted based on reactant concentration. The results of these experiments are shown in Figure 4.10 and Figure 4.11.

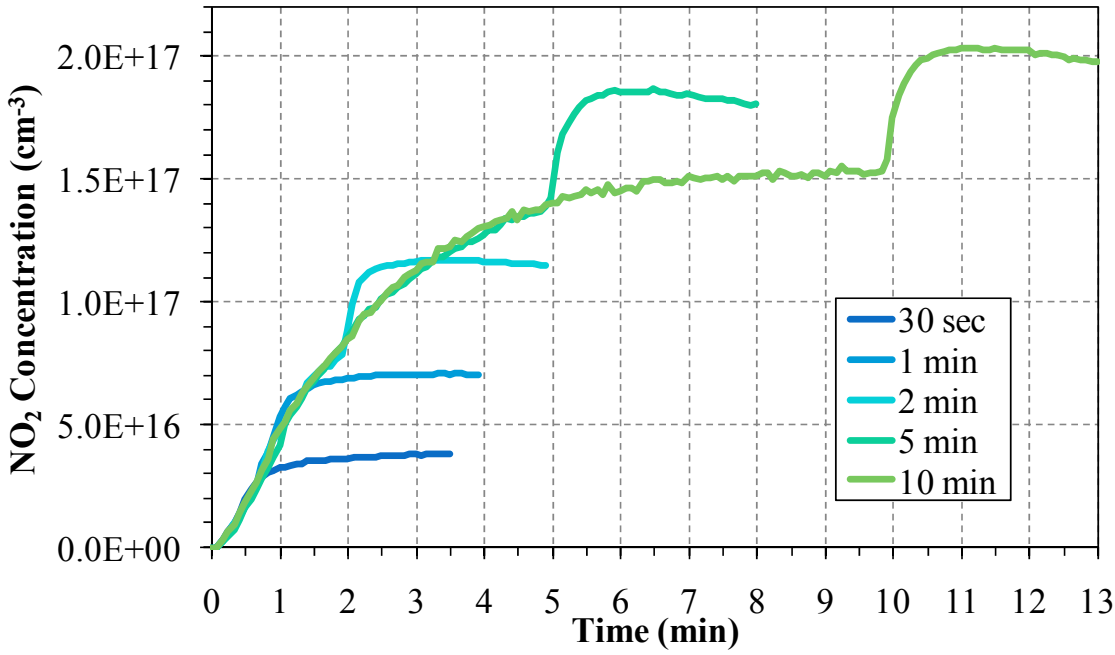

Figure 4.10. NO_2 formation in the plasma flame at a gas mixing ratio of 1N:1O.

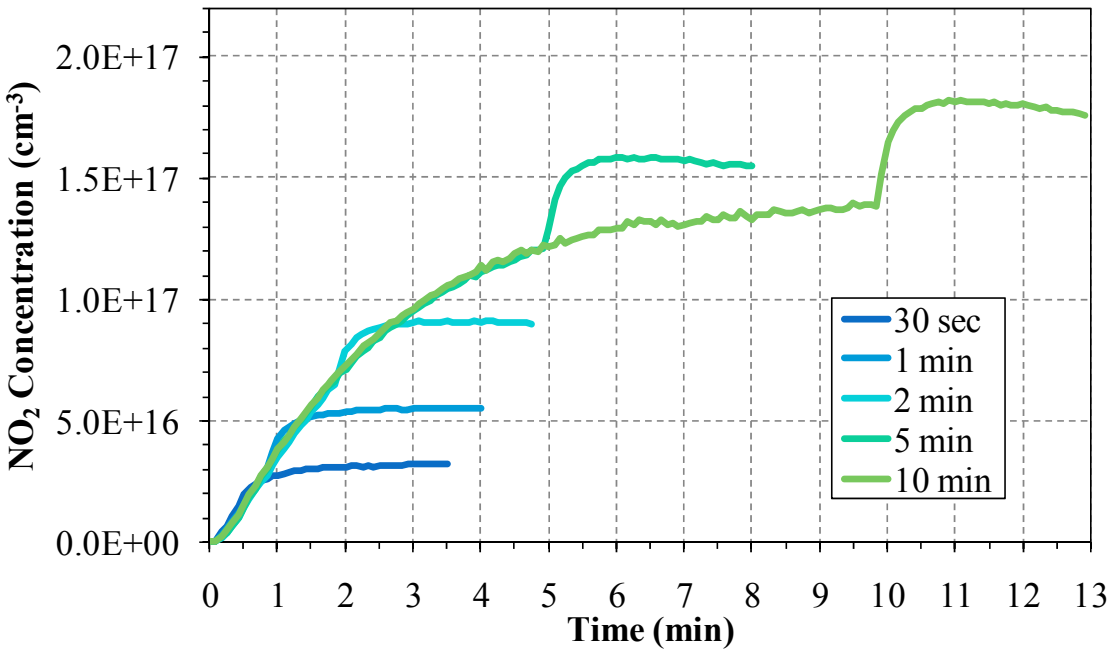

Figure 4.11. NO_2 formation in the plasma flame at a gas mixing ratio of 1N:4O.

The highest concentration of NO_2 was found with the gas mixing ratio 1N:1O at the longest plasma reaction time. This is most likely the case because it represents the composition closest to a proper stoichiometric ratio. In addition to differences in final NO_2 concentration, the rates of formation are also different for each gas ratio. The ratio 4N:1O has a consistently higher rate than the other two. Since the rate is higher for 4N:1O, this concentration generates the highest NO_2 concentrations at the shorter reaction times. The gas mixing ratio 1N:4O generated the lowest levels of NO_2 and also had the slowest reaction rate.

As mentioned above, one of the most interesting features of this process is the fact that the NO_2 concentration increases by 30-60% once the plasma is turned off. Initially, this was suspected to be a result of active species with long lifetimes, since metastables can have a relatively long lifetime at atmospheric pressure [49]. This turns out not to be the case, however, since the concentration increase takes place over tens of seconds rather than milliseconds or seconds. The basis for this phenomenon actually comes from the effect temperature has on the discharge.

4.3.4 Thermal Effects

The gas temperature within the plasma is important in its ability to control chemical reactions. As was discussed in section 2.4, this temperature can be ascertained from the shape of a rotational emission band; in this case the OH band at 306-311 nm. The program LIFBASE [19] provides simulated spectra of various molecules which can be matched to an experimental spectrum based on temperature.

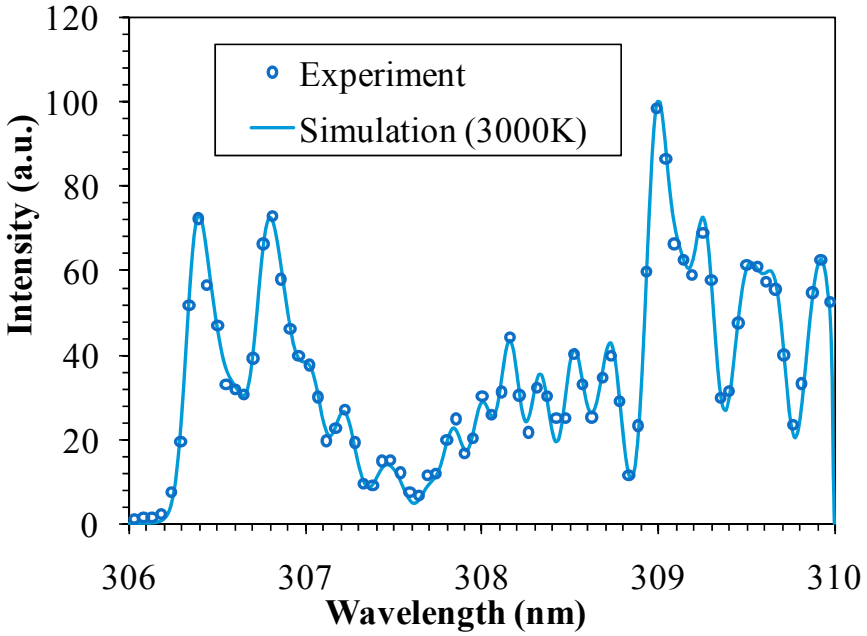

Figure 4.12. Comparison of OH emission from experiment and simulation at 3000K.

Figure 4.12 shows the results of a simulation at 3000K in comparison to the experimental spectrum, and the two agree to within 5%. This temperature is consistent with other low current arcs [68] and is on the high end of the range for non-equilibrium plasmas [26]. The plasma flame's temperature (electron and gas) and coupled excitation mechanisms (thermal gas heating associated with thermal discharges, electronic excitation associated with non-thermal discharges) allow for formation of species which have large activation barriers. The utility of this discharge can be understood from the following example.

Imagine a plasma process which requires dissociation of CO_2 (e.g. carbon sequestration from flue gases). Carbon dioxide can be hard to dissociate because of its high bond energy (5.5 eV). If a purely thermal discharge is used in this process, a temperature of over 63,000

K (1 eV = 11604 K) would be required for complete dissociation of CO_2! This problem is often overcome by utilizing non-thermal discharges, where electrons in the high energy tail of the EEDF promote stimulated vibrational excitation. This specific coupling into carbon dioxide's vibrational modes—as opposed to the lack of mode-specific energy transfer associated with thermal discharges—effectively generates CO and O. But what about the reaction rate? As always, this is strongly affected by the temperature of the interacting species: electrons, ions, neutral gas molecules or metastables. Therefore, the electron energy may be sufficient enough to stimulate dissociation, but the reaction rate may be low because the temperature of the feed gas is too low (gas molecules in non-thermal discharges often operate near room temperature). As such, a discharge is required which has both a relatively high gas temperature and an even higher electron temperature—in other words, a hybrid thermal/non-thermal plasma like the plasma flame is needed.

The foregoing example provides a framework for understanding NO_2 generation with the plasma flame. In general, NO_2 formation is known to be sensitive to changes in temperature. Reactions which produce NO_2 become kinetically unfavorable at high temperatures, as is the case with ozone (O_3). It is therefore important to investigate the temperature differential between the plasma and the surrounding environment. The ambient gas temperature inside the reactor was measured as a function of time for various plasma reaction times at a gas mixing ratio of 4N:1O and is shown in Figure 4.13. The noise seen on the 5 min and 10 min

runs can be attributed to spatial variations in the position of the discharge while measurements were taken.

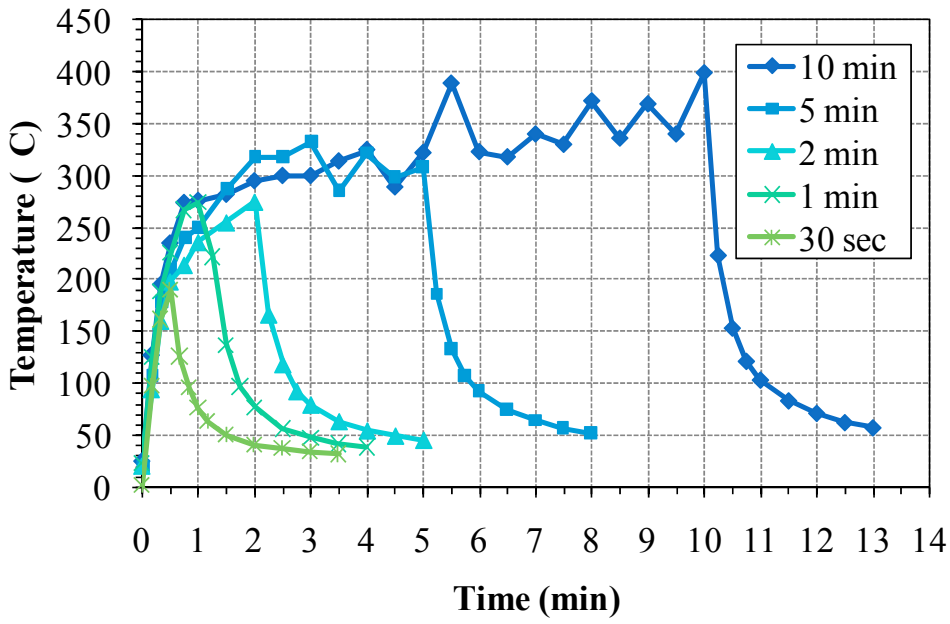

Figure 4.13. Temperature of the ambient gas inside the reaction chamber for various plasma reaction times. The gas mixing ratio for this data was 4N:1O.

For all plasma reaction times, the ambient gas temperature increases drastically within the first minute and, for the 5 and 10 min runs, reaches equilibrium at approximately 300-350^{o}C. Once the plasma is extinguished the temperature drops exponentially over the course of 1-1.5 min.

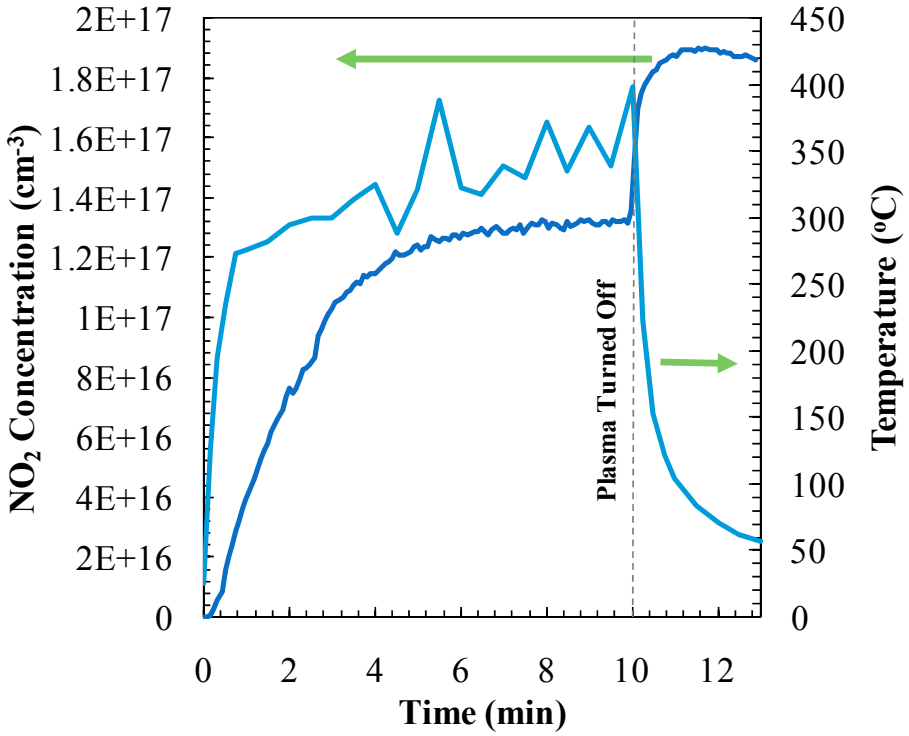

Figure 4.14. Comparison of NO_2 concentration and ambient gas temperature with a 10 min plasma reaction time and a gas mixing ratio of 4N:1O.

When this phenomenon is compared to NO_2 formation (Figure 4.14), it is clear that the ambient gas temperature *decreases* exponentially as the concentration *increases* exponentially on approximately the same time scale. Given the negative dependency of NO_2 synthesis on temperature, the increase in NO_2 concentration can be explained by the decrease in ambient gas temperature. In other words, a balance exists between formation and destruction of NO_2 and this balance is controlled by temperature. The extent to which temperature plays a role in reaction kinetics will be explored further in Chapter 5.

4.4 Conclusions

The plasma flame has been characterized in terms of its electrical properties, its propensity for generating active species and NO_2, and its thermal properties. It was found that the discharge is a hybrid plasma which has the capability of being chemically active at temperatures which are significantly higher than typical non-thermal discharges.

Significant levels of NO_2 synthesis have been shown using the plasma flame. It was also found that active species facilitate NO_2 formation reactions when the plasma is on, but heat losses control the reaction pathways once the discharge is off. External temperature control will likely allow for increased production efficiency. The next chapter will investigate the role of atomic oxygen, input power, and plasma temperature on NO_2 formation.

5 Effect of Atomic Oxygen on NO_2 Production

5.1 Introduction

Atomic oxygen is one of the most active species in nature. So active, in fact, that at atmospheric pressure it rarely exists for longer than a fraction of a second. It will quickly and effectively act to oxidize nearly any material or compound. In the upper portion of the earth's atmosphere where atomic O is formed via high energy radiation (e.g. solar winds), it is even known to cause substantial corrosion in satellites and related apparatus [69]. In the context of non-equilibrium air plasmas, atomic oxygen accounts for much of their chemical reactivity. It is important, then, to understand the role it plays in NO_2 formation.

NO_2 synthesis using the plasma flame was introduced in Chapter 4. It was experimentally determined that NO_2 formation can be correlated with the ambient gas temperature. This chapter will compare the results from Chapter 4 to a kinetic model established in the literature to develop a fundamental understanding of the underlying reaction mechanisms. These mechanisms are further probed by studying the effect processing variables have on the concentration of atomic oxygen. The goal of this research is to develop a complete understanding of the interaction between process variables, plasma and ambient gas temperatures, reactant populations and NO_2 synthesis.

5.2 Experimental

The experimental reactor and measurement setup were described in Chapter 3. For these experiments, the reactor was filled with some ratio of nitrogen to oxygen (4N:1O, 1N:1O, 1N:4O) and a continuous flow was maintained throughout the experiments. This created a steady state environment in which significant changes in gas chemistry were prevented while the measurements were taken.

Both applied power (30-100 W) and driving frequency (159 and 105 kHz) were varied to determine their effects on atomic O emission. The driving frequency 159 kHz is the most stable operating frequency for the discharge, but is not the principle coupling harmonic for the transformer and power supply. When using this frequency, the applied power—and specifically current—is limited by a reduced coupling efficiency between the power supply and the plasma. On the other hand, 105 kHz is the principle coupling harmonic of the power supply. Efficient power transfer associated with this frequency generates a more energetic discharge. Therefore, even though the chosen frequencies are similar in magnitude, they represent different modes of operation for this power supply and discharge. The power range above was covered for each frequency and gas composition, and the experimental parameters of the data set are outlined in the table below.

Table 5.1 *Experimental outline including driving frequency (kHz), power (Watts; H-high, M-medium, L-low) and nitrogen to oxygen gas mixing ratio.*

Run #	Frequency	Power	N:O
1	158	H	4:1
2	158	M	4:1
3	158	L	4:1
4	100	H	4:1
5	100	M	4:1
6	100	L	4:1
7	158	H	1:1
8	158	M	1:1
9	158	L	1:1
10	100	H	1:1
11	100	M	1:1
12	100	L	1:1
13	158	H	1:4
14	158	M	1:4
15	158	L	1:4
16	100	H	1:4
17	100	M	1:4
18	100	L	1:4

Atomic O emission at 777 nm was measured for each run. The emission profile at this wavelength is actually superimposed onto a broadband emission profile (Figure 5.1).

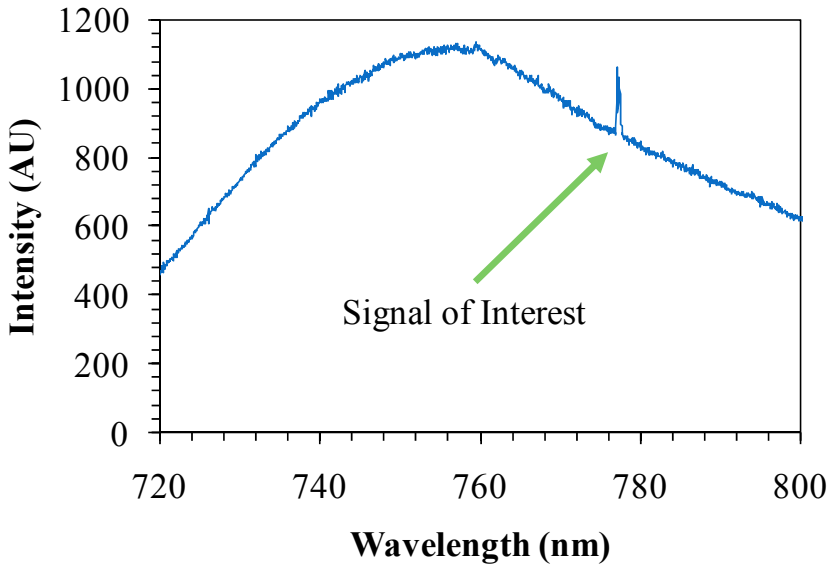

Figure 5.1. Emission from run 13 (1N:4O, 158 kHz, high power).

To extract the signal of interest, the following procedure was used (Figure 5.2). First, a middle Riemann sum was calculated for the intensity from 777-778nm as

$$A_O = \sum_n \left(\frac{I_n - I_{n-1}}{2} \right) \left(\lambda_n - \lambda_{n-1} \right) \tag{5.1}$$

where the integrated atomic oxygen signal A_o is the sum of n elements whose areas are defined by the width λ_n-λ_{n-1} and height $(I_n$-$I_{n-1})/2$. The width of each element was defined by the wavelength position of each pixel in the channel, which gave an average width of 0.045 nm. The total window width of A_O was 1 nm. The value of A_O represents the signal of interest plus an unknown level of background radiation.

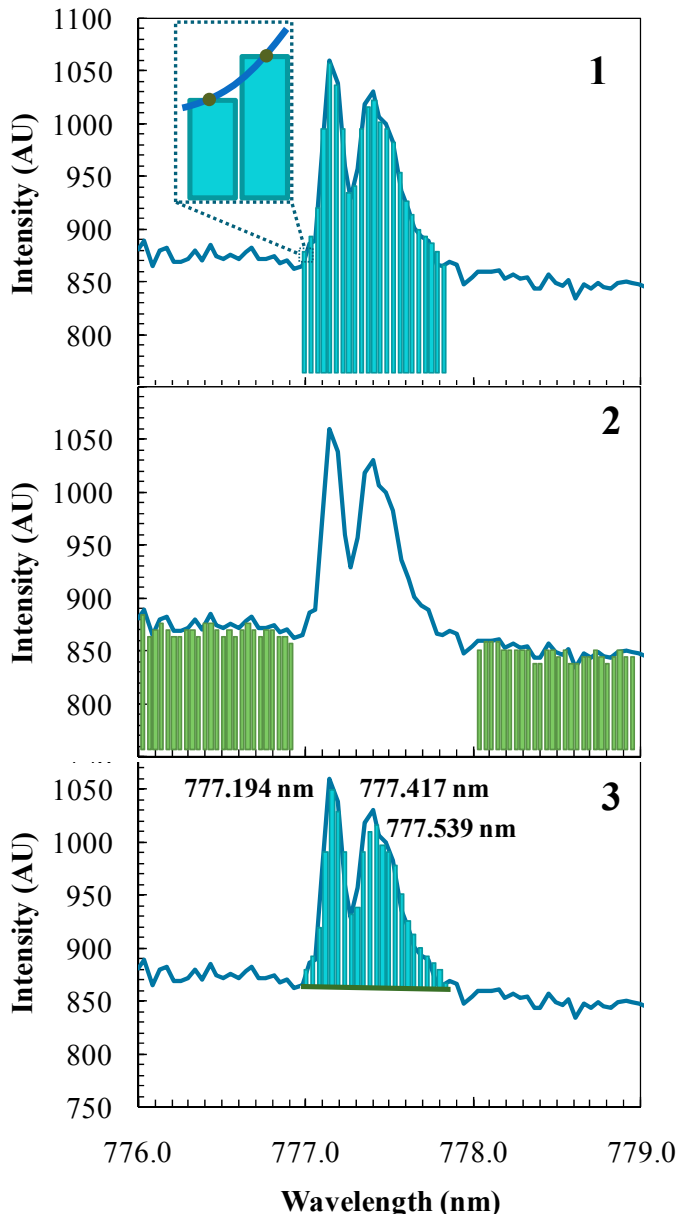

Figure 5.2. Data processing technique for extracting atomic O signal from background radiation. Step 1: Reimann sum calculation for desired signal from 777-778 nm using the midpoint approximation (inset). Step 2: Reimann sum calculation for broadband emission from 776-777 nm and 778-779 nm. Step 3: Average integrated intensity of broadband emission and subtract from Step 1 to leave only O emission.

After finding A_O, the second step was to evaluate the intensity of background radiation A_b, which was calculated using equation (5.1). A_b was calculated for a 1 nm window width on either side of A_O, i.e. 776-777 nm and 778-779 nm. The element width was the same as with A_O, 0.045 nm. The final step of this process was to compute the average of the two A_b values and subtract it from A_O. The values obtained from this process provide a relative indication of atomic O population for each process condition and therefore basis for comparison. Every collected spectrum was an average of 10 spectra, each with an integration time of 2 seconds.

The gas temperature within the plasma was determined as a function of power using OH emission (306-311 nm) and LIFBASE [19]. The temperature was varied until the peak correlation coefficient converged on a maximum value. This represented the best fit simulation, with an error of approximately 5%.

5.3 Results and Discussion

5.3.1 Reaction Kinetics and NO_2 Formation

A kinetic model for the chemistry of air plasmas at atmospheric pressure has been established in the literature [48]. Based on this model, reactions pertinent to NO_2 generation are as follows:

Table 5.2 *Reaction list for NO_2 formation.*

	Reaction
1	$NO + O + M^a \rightarrow NO_2 + M^a$
2	$NO_2 + M^a \rightarrow NO + O + M^a$
3	$NO_2 + NO_2 \rightarrow NO + NO + O_2$
4	$NO + NO + O_2 \rightarrow NO_2 + NO_2$
5	$NO_2 + O \rightarrow NO + O_2$
6	$NO + O_3 \rightarrow NO_2 + O_2$

[a]M denotes a third body, e.g. N_2, O_2, or NO.

The reaction rate coefficient k for these reactions, calculated from an Arrhenius relationship, is extremely sensitive to temperature fluctuations. This is especially true for the temperature range in which the present discharge operates. Temperature dependencies for the rate coefficients can be seen in Figure 5.3.

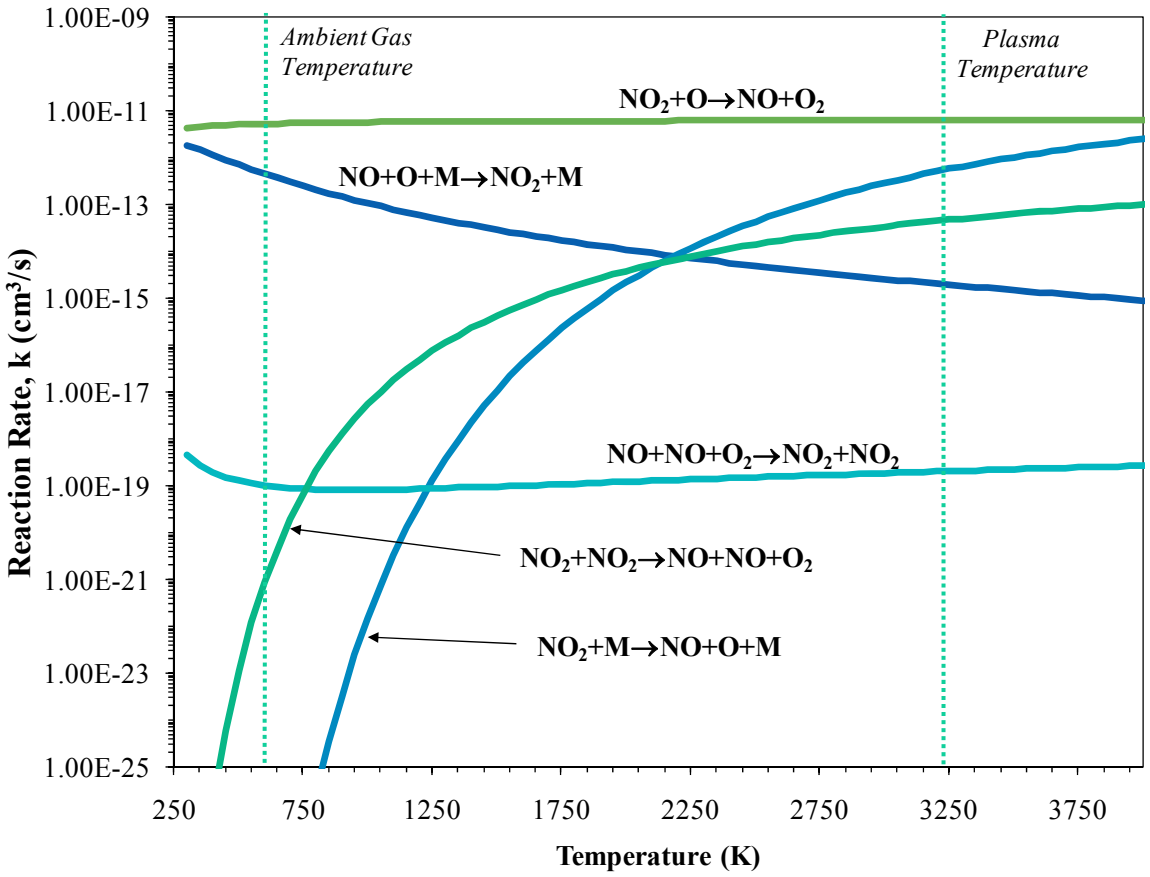

Figure 5.3. Temperature-dependent reaction rates k for reactions 1-6 with special note of the ambient gas temperature and plasma temperature.

As mentioned before, NO_2 formation and destruction is extremely temperature dependent. This is easily seen in Figure 5.3. Reaction 5 dominates by several orders of magnitude in the temperature range shown; however, even though this reaction is very fast it is limited by the population of atomic O. Therefore, as O reacts to form NO_2 via reaction 1, reaction 5 will not facilitate further destruction of NO_2.

The three-body reactions 1 and 2 play a dominant role in NO_2 generation. This is due to the well known, highly collisional nature of atmospheric pressure plasmas, in which reactions are dominated by neutral-neutral interactions and relevant three-body reactions [49, 70]. As a result, the energy of ambient gas within the reaction chamber plays a substantial role in determining whether pertinent reactions are product-driven or reactant-driven.

Another important point to note is the difference between the ambient gas temperature and the plasma temperature—600 K and 3300 K, respectively. When these values are outlined on the kinetic plot, it is clear that the dominant reactions inside the plasma and outside the plasma are different. In particular, the high temperature of the plasma drives the destruction of NO_2 via reactions 2, 3 and 5, whereas the reduced temperature of the surrounding gas facilitates the formation of NO_2 via reaction 1. The discharge itself can then be considered as a "factory" for active species (NO, O, etc.) which react to form NO_2 once they diffuse outside the plasma.

It should be noted that reaction 6 is not shown in Figure 5.3 for two reasons. First, atomic O is needed to form both O_3 and NO_x, so the formation reactions for each actually compete. Nitrogen oxides tend to form in air plasmas rather than ozone since O has such a higher affinity to nitrogen than it does to O or O_2, i.e. nitrogen oxides have higher bond strengths than O_2 and O_3. The concentration of O_3 is therefore very low in the presence of N_2. The second reason reaction 6 is not shown is because its rate is at least 10^{18} times higher than reactions 1-5. Since O_3 tends to form in air plasmas only at low levels, the population

formed initially is destroyed so quickly via reaction 6 that it is not available on an appreciable time scale.

Since atomic O is so pervasive in this discharge, the next section will evaluate the relative abundance of O for different experimental conditions. This will then be correlated to NO_2 production.

5.3.2 Effect of Power and Frequency

When comparing the plasma flame in different gas mixing ratios, it is clear that the discharge operates in very different modes for each composition. Figure 5.4 shows a comparison of the functional dependency of plasma current on applied power for the three gas mixing ratios.

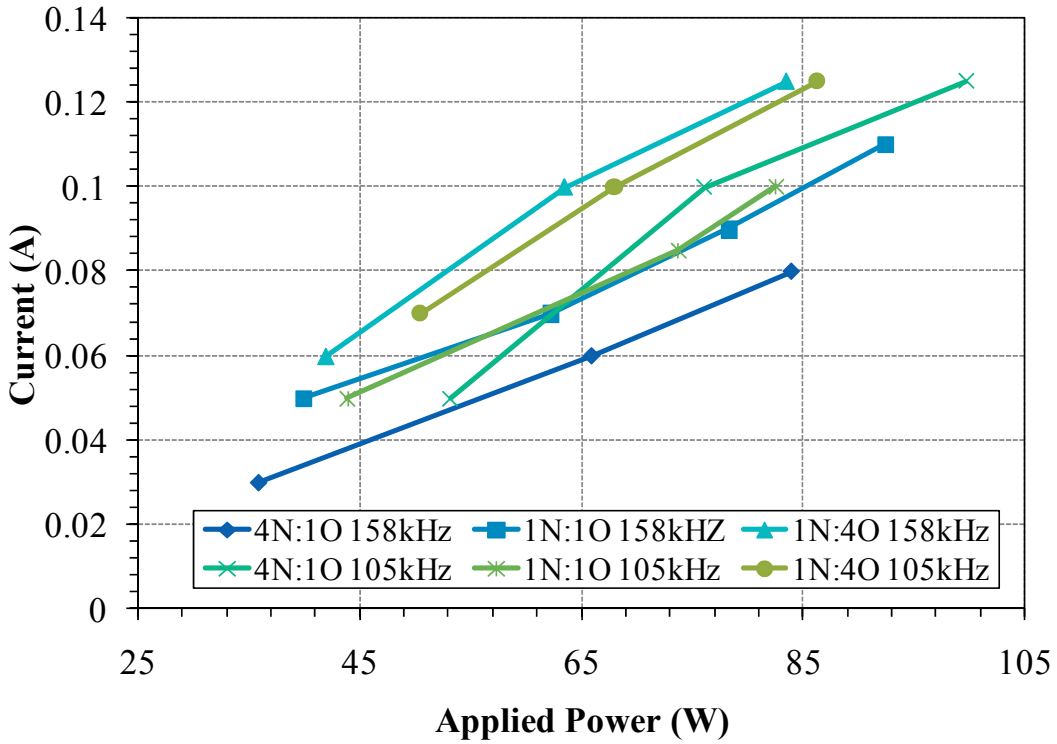

Figure 5.4. Effect of gas composition on current drawn by the discharge.

For both frequencies, the 1N:4O group drew significantly more current than their counterparts at the same frequency—as much as 0.45 A more. This effectively produced a discharge which was very intense, where the thermal core expanded to fill nearly the entire plasma volume. Moreover, even the 1N:1O group drew more current than the 4N:1O group; therefore, the addition of oxygen leads to larger currents at a given power. The low current associated with 4N:1O is most likely associated with the high dissociation energy of diatomic nitrogen (9.8 eV). That is, more energy is spent on vibrational excitation when excess nitrogen is present. The dissociation energy of diatomic oxygen, in contrast, is only

5.16 eV; therefore, the energy not consumed by vibrational excitation contributes to Joule heating. The energy cost of N_2 dissociation is so high that in 4N:1O the plasma temperature essentially remains constant for the power range studied here (Figure 5.5).

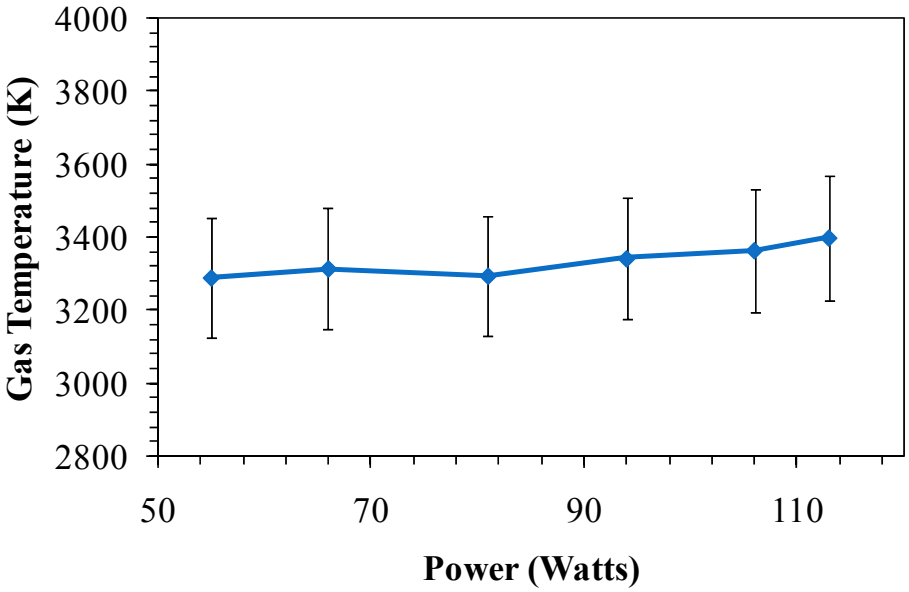

Figure 5.5. Gas temperature within the plasma for different power levels with a gas mixing ratio of 4N:1O.

The effect of power, gas mixing ratio and driving frequency on atomic O production can be seen in Figure 5.6 and Figure 5.7. The effect of frequency on O emission is negligible, despite the fact that at 105 kHz the discharge draws more current for each of the gas mixing ratios (Figure 5.4). While current plays a large role in plasma chemistry and plasma temperature, there is not enough difference in current between the two frequencies to facilitate an appreciable change. In contrast, a large difference in current exists between the gas mixing ratios—that is, 1N:4O drew the most current at both frequencies and 4N:1O drew

the least. Given the different behaviors of oxygen- and nitrogen-rich air plasmas described above, these large differences in current should lead to differences in reaction chemistry. This turns out to be true. A weak functional dependence between O emission and power can be seen for gas mixing ratios 4N:1O and 1N:1O. O emission in the oxygen-rich mixture, on the other hand, exhibits a strong dependence on power. This could be caused by two factors.

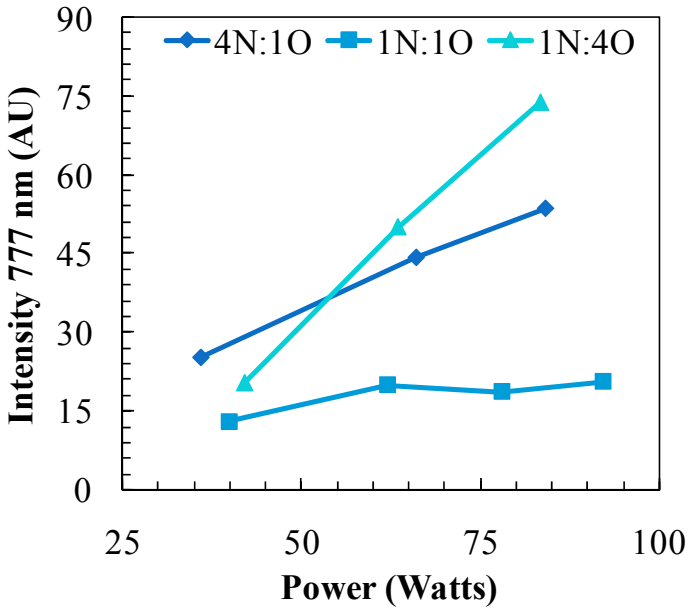

Figure 5.6. Atomic O intensity for different powers and gas compositions. Driving frequency was 158 kHz.

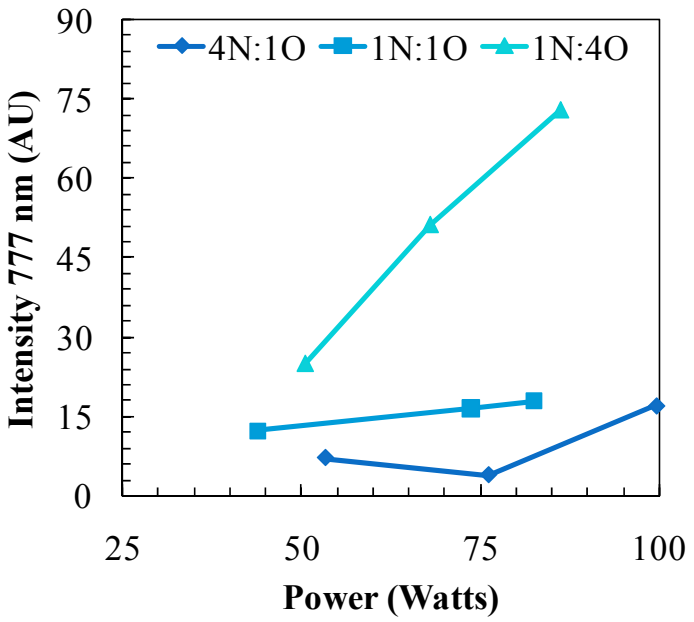

Figure 5.7. Atomic O intensity for different powers and gas compositions. Driving frequency was 105 kHz.

First, operation in a more "thermal mode" requires the necessary dissociation energy to come from conventional gas heating rather than electronic- or metastable-stimulated dissociation. An increase in power would increase the temperature and therefore the level of O_2 dissociation would increase. Second, since the ambient gas temperature should increase with power for 1N:4O, the NO_2 forming reactions will be less dominant. This is tied into the reaction rates shown in Figure 5.3. With less O being consumed to form NO_2, its population inside the plasma will be higher and hence more emission will be observed. This would explain why the O emission remains nearly constant with power for 4N:1O and 1N:1O. Since the temperature remains consistent as power is varied, the number of O atoms reacting

to form NO_2 should remain constant in the plasma and the measured emission should stay the same as well.

This leads to an important point about O emission in the plasma flame. It appears that a negative dependency exists between O emission and NO_2 formation. That is, higher levels of O emission indicate less NO_2 synthesis and vice versa. This is related to the fact that if O is consumed to form NO_2 it will not be available for excitation in the plasma.

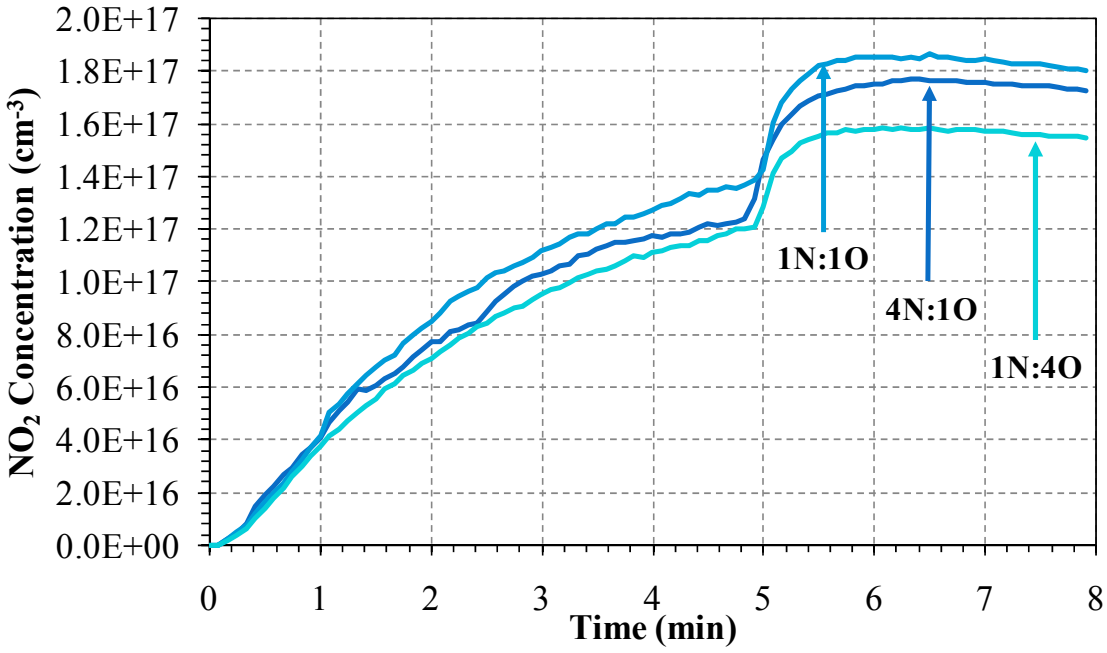

Figure 5.8. NO_2 concentration as a function of time for various gas mixing ratios. The plasma reaction time is 5 min, the applied power is 90 W and the driving frequency is 158 kHz.

Figure 5.8 shows the NO_2 concentration as a function of time for various gas mixing ratios at 90 W and 158 kHz. When comparing the final concentration of NO_2 to O emission in Figure 5.6, it is clear that the negative dependency is followed.

5.4 Conclusions

The effect of O emission on NO_2 generation was investigated, in addition to the role of power and driving frequency on O emission. The role of frequency was determined to be negligible for all gas mixing ratios. Power has a significant effect for 1N:4O, but has little to no effect for 4N:1O and 1N:1O. The influence of power in the 1N:4O gas mixture can be understood by looking to the nature of the reactants in the discharge. That is, the relatively lower bond energy of diatomic oxygen facilitates less energy consumption by vibrational excitation, thereby providing an energy surplus for gas heating. These higher temperatures lead to NO_2 destruction, as was determined from a theoretical kinetic analysis. NO_2 destruction (or lack of NO_2 formation) means excess atomic O is present in the discharge and hence more O emission is seen.

It is clear that gas temperature plays a huge role in plasma chemistry. By controlling the ambient gas temperature and plasma temperature, one could presumably design an environment where dominant reaction pathways are specifically chosen for the application of interest. This is a very powerful feature of hybrid discharges, and is a hallmark of the plasma flame.

6 The "Plasma Flame" and Its Applications

6.1 Introduction

Operating principles behind the plasma flame were covered in chapters 4 and 5. This knowledge can be utilized for a variety of engineering applications, including printed circuit board (PCB) fabrication, biofuel production and formation of syngas. The breadth of applications presented here is intended to show how the plasma flame can be easily implemented into processes which require basic chemical functionality at low cost and high energy efficiency. By simply changing the input gases, applied power and gas temperature, it is feasible to envision a huge number of applications in which the plasma flame would excel.

6.2 Experimental

6.2.1 "Acid on Demand" Setup

The experimental setup described in section 3.1 was used, with a few modifications (Figure 6.1). Rather than operating in a static flow environment, gas flow was introduced with a mixing ratio of 4N:1O. The system exhaust was then bubbled through 100 mL deionized water. The goal of this setup is to react the NO_2 with water to generate HNO_3.

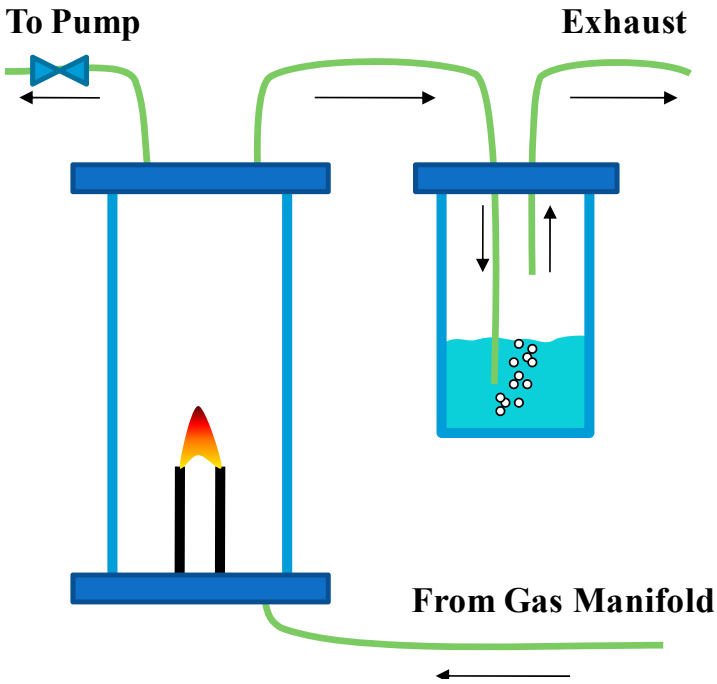

Figure 6.1. Schematic of modified experimental reactor. A bubbler was added for formation of HNO_3.

Furthermore, the bubbler was placed in an ice bath in order to increase the solubility of NO_2 in water. This design would allow a heat exchanger to be used in place of the ice bath to increase process efficiency. By cycling the heat back into the reactor to raise the ambient gas temperature, less power could be used to obtain the same concentration of NO_2. That is, less power would be needed for dissociation of N_2 and O_2.

The plasma was ignited for a certain period of time (30 sec, 2 min, 5 min or 10 min) at a power of 70 W, after which the pH of the water was tested using an Orion Model 301 pH meter. For a copper etching experiment, a 2 cm x 4 cm x 0.1 cm piece of bulk copper was added to the acidified water. To show the applicability of "Acid on Demand" to the

microelectronics industry, a mask was fabricated from electrical tape and placed on the copper sample.

"Acid on Demand" was also used as a method for degrading southern pine wood chips. This process would generate sugars which can be fermented to make ethanol. The experimental setup is similar to the one used for copper etching, except southern pine chips (0.85-2 mm size) are placed at the bottom of the bubbler. No water was added to the wood chips since they inherently contain a sizeable portion of water (10-50%). In other words, the acid can be formed *in situ*. The setup is shown in Figure 6.2.

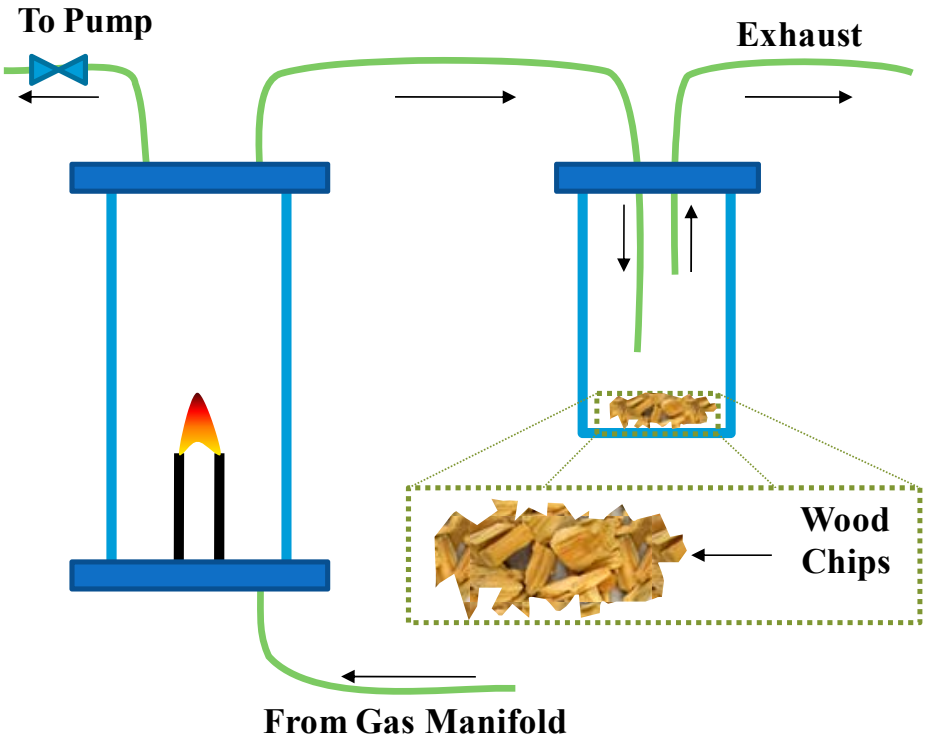

Figure 6.2. Experimental setup for biomass hydrolysis.

A gas mixing ratio of 4N:1O was used with a plasma reaction time of 10 min at 158 kHz and 90 W. The gas flow was maintained for 20 minutes after the plasma was turned off. This provided the maximum interaction between the NO_2 generated and the biomass. Samples were treated by experimental recipe seen in Figure 6.3.

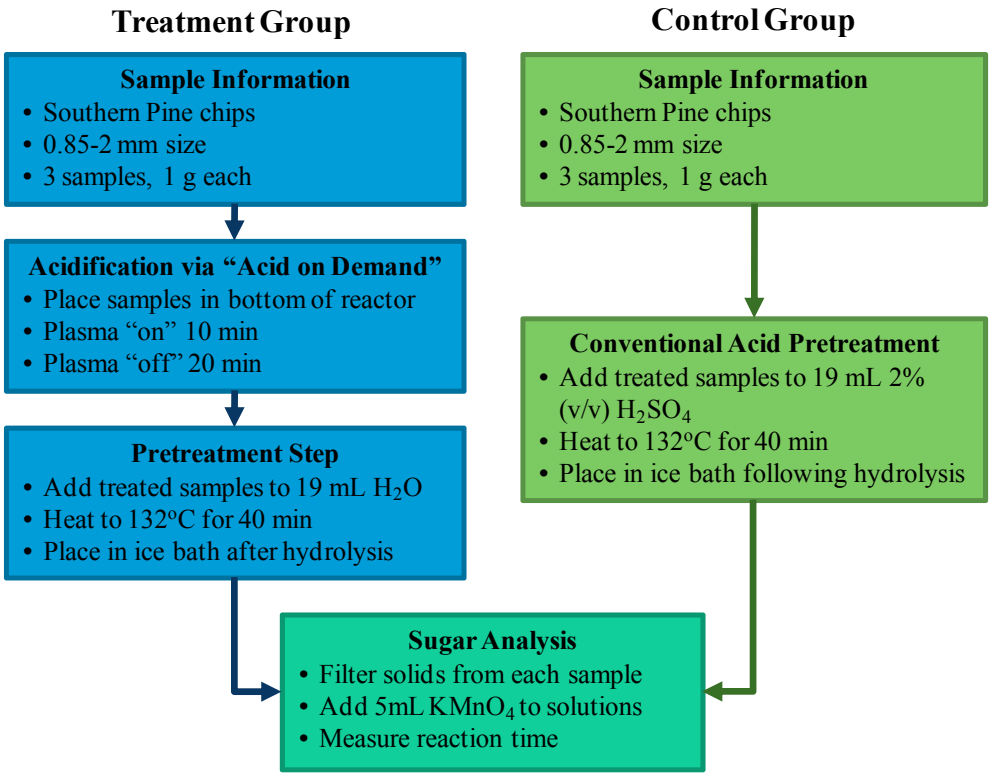

Figure 6.3. Experimental outline for "Acid on Demand" treatment of biomass.

Once the samples were treated in the reactor, they were added to 19 mL deionized water and placed in an oven at 132°C for 40 minutes. This step will allow the HNO3 created during the "Acid on Demand" process to penetrated into the wood chips' structure. A set of control samples was also created, where 1 gram (3 replicates) of southern pine chips were

added to 19 mL 2% (v/v) H_2SO_4 and placed in an oven at 132°C for 40 minutes. Once taken out of the oven, both treated and control groups were placed in an ice bath for 5 minutes to quench unwanted reactions. Filter paper with a 25 μm pore size was then used to separate the solids from the filtrate.

The procedure for measuring the presence of fermentable sugars utilizes the reduction of potassium permanganate (a purple-pink indicator) with hydrogen ions obtained from the sugars, i.e. $MnO_4^- + 8H^+ + 5e^- \rightarrow Mn^{2+} + 4H_2O$ [71]. The permanganate reacts with the sugars in solution to produce a colorless compound; therefore, more sugars leads to faster loss of color. The amount of time required for the solution to lose its color indicates how effective the acid hydrolysis process is at breaking down the biomass. Therefore, if "Acid on Demand" is an effective pretreatment, the reactions of the treated samples will go to completion faster than the untreated samples.

6.2.2 Syngas Production Setup

In order to generate syngas using the plasma flame, a mixture of CH_4, H_2O and Ar was used. The methane was bubbled through water at a flow rate of 250 sccm. The water was heated to 50°C to increase its vapor pressure. Argon was used as a carrier gas at a flow rate of 2 slm. The applied power was maintained at 90 W, and the two applied frequencies were 158 kHz and 50 kHz.

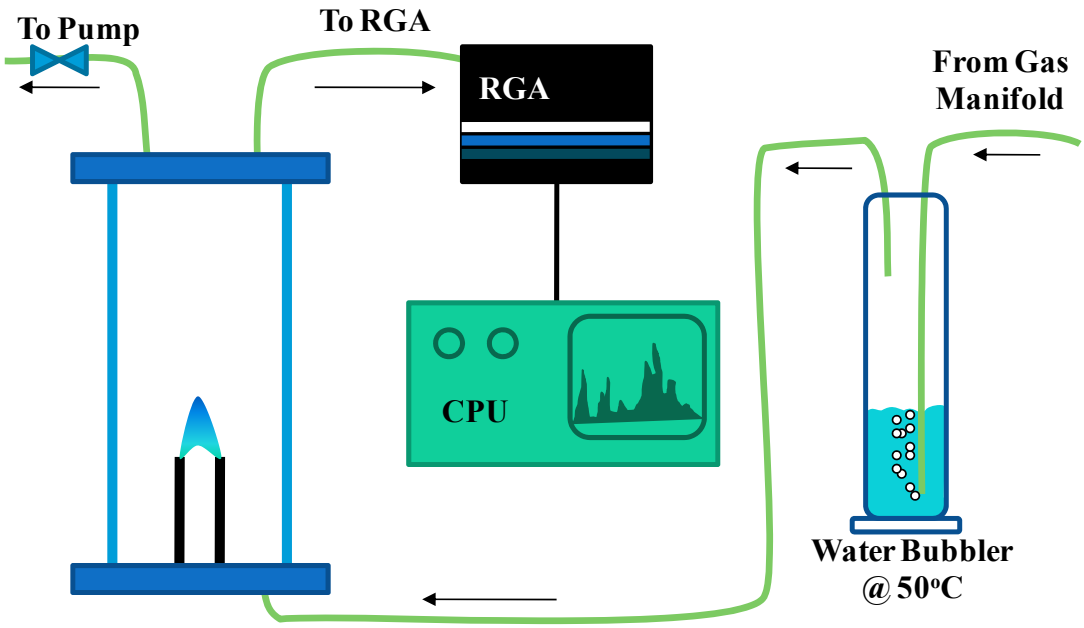

Figure 6.4. Setup for generation of syngas ($CO+H_2$) from methane and water (CH_4+H_2O).

The reactor exhaust was analyzed with a residual gas analyzer (MKS Spectra Products "VAC-CHECK"). The following masses were analyzed (included in parentheses are compounds corresponding to that mass number and the color of that mass number in the data shown in section 6.4): 1 (H; purple), 2 (H_2; red), 12 (C; pink), 14 (N, CH_2; blue), 16 (O, CH_4; yellow), 17 (OH; dark green), 18 (H_2O; turquoise), 28 (N_2, CO; light green), 32 (O_2; black), 40 (Ar; white), and 44 (CO_2; teal).

6.3 "Acid on Demand"

6.3.1 Reduction of pH for Different Reaction Times

It is well known that NO_2 is soluble in water and will also react to form HNO_3 via the reaction $4NO_2 + 2H_2O + O_2 \rightarrow 4HNO_3$. The purpose of this section is to evaluate the plasma

flame's effectiveness in producing HNO_3. The reduction of pH as a function of reaction time using the experimental setup seen in Figure 6.1 is shown in Figure 6.5. This is taken as an indication of HNO_3 formation.

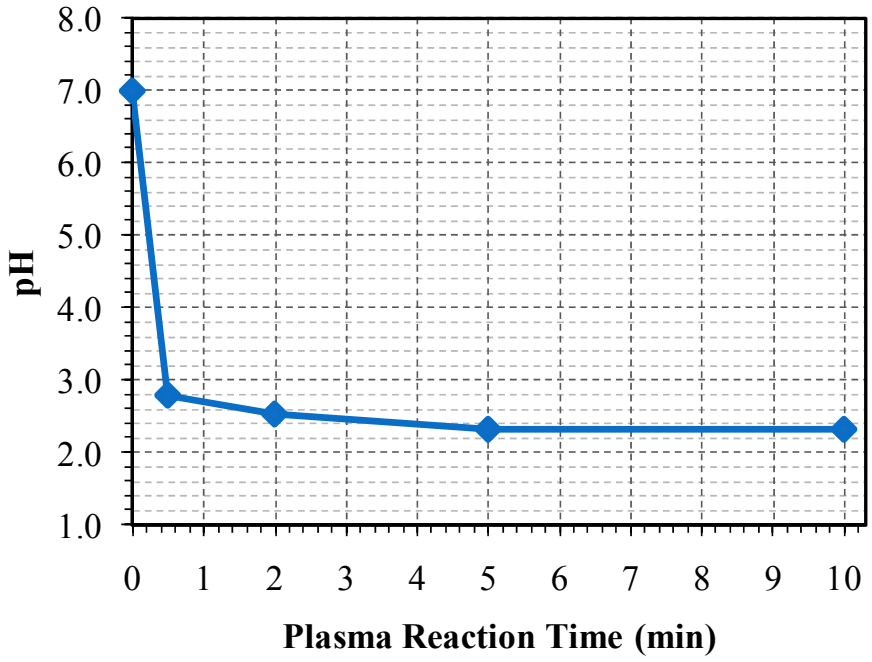

Figure 6.5. Reduction of pH as a function of time when reacting NO_2 created by the plasma flame with water.

The pH of the water is quickly reduced and reaches a minimum of 2.3-2.5 at around 2 minutes. This lower limit is most likely a result of the interaction between NO_2 solubility in water and the availability of O_2 to complete the reaction listed above. Further improvements could be made by adding excess O_2 to the bubbler, and by subsequently distilling the HNO_3

to a higher concentration. Some processes may not need such a concentrated acid, however, so the "Acid on Demand" process as it stands would suffice.

6.3.2 Acid on Demand for Microelectronics

Since the "Acid on Demand" process has been shown to be effective for producing HNO_3, it can presumably be utilized in any process which requires HNO_3. One such process is the etching of copper for microelectronic devices. Copper is often used for leads or interconnects between components on a printed circuit board (PCB), given its high electrical conductivity. Conventional processes for patterning interconnects include either mechanical or chemical means, i.e. milling or etching.

Bulk copper (Figure 6.6) was patterned and etched using the "Acid on Demand" process as a means of replacing conventional etching processes. The results of etching are shown in Figure 6.7.

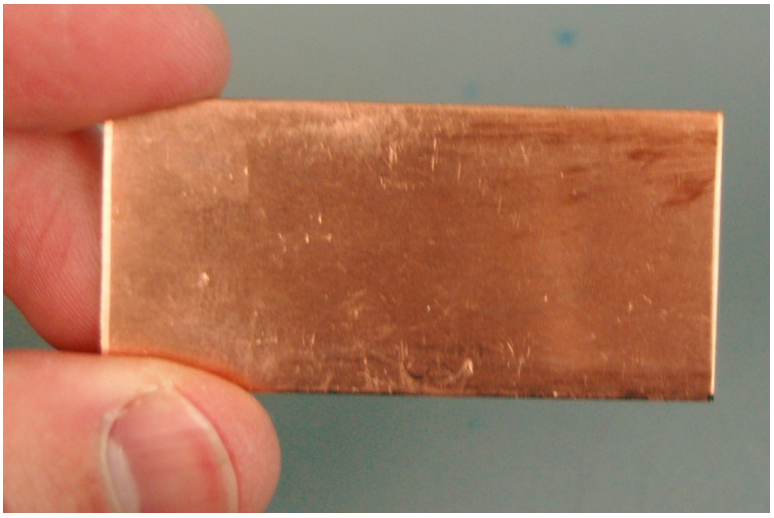

Figure 6.6. Bulk copper sample prior to patterning and etching.

Figure 6.7. Bulk copper sample following "Acid on Demand" etching.

Clearly, the acid produced via the "Acid on Demand" process can be used for patterning copper and hence can be developed for the microelectronics industry. Full scale implementation of this process would allow for continuous acid production on-site at the PCB fabrication facility.

6.3.3 Acid on Demand for Biofuel Production

There has been a multitude of research conducted in the area of lignocellulosic materials—i.e. corn stover and wood chips—in the past few decades [72]. The ultimate goal of this research is to develop processes which remove the lignin and convert the cellulose and hemicellulose polymers into fermentable sugars. These sugars can then be used, among other things, to make ethanol.

The process most commonly used—and most thoroughly researched—is enzymatic hydrolysis. Enzymatic hydrolysis utilizes enzymes to selectively break down the polysaccharides without generating unwanted byproducts. In order for the enzymes to be effective, however, the biomass must be pretreated in some manner. The most common pretreatment utilizes a dilute acid. There are different techniques associated with the type of acid used and the concentration of the acid. Concentrated acid involves short reaction times, but requires a corrosion resistant vessel and a method for recycling the acid. Dilute acid is lower in cost and produces fewer unwanted byproducts, but requires a longer residence time. In spite of that, dilute acid pretreatment stands as the most common method to date. A common acid used in these processes is sulfuric acid (H_2SO_4). Here a process is presented which can generated another important acid (HNO_3) for biomass pretreatment and ultimately ethanol production. The acid can be generated on-site, which is a great advantage over conventional technologies that require acid transportation and handling.

Results from the procedure outlined in Figure 6.3 can be seen in Figure 6.8 and Table 6.1. It is clear that the "Acid on Demand" group produced significantly more sugars than the conventional treatment. In fact, the conventional treatment samples were unable to completely reduce the $KMnO_4$ in solution; monitoring of the reaction was discontinued after 2 min, at which point the color of the solutions were no longer changing.

Table 6.1 Results from hydrolysis experiments.

	Sample #	Time required to reduce all $KMnO_4$
"Acid on Demand" Pretreatment	1a	46
	1b	53
	1c	48
Conventional Acid Hydrolysis	2a	> 2 min
	2b	> 2 min
	2c	> 2 min

The solutions of the two sample groups themselves also present differences in color (Figure 6.8). The samples at the top of the figure ("Acid on Demand" samples) show a darker color representative of more thorough degradation. Specifically, the compounds which cause such color are typically associated with degradation products from lignin. This is a positive result, as lignin is a major inhibitor to efficient hydrolysis.

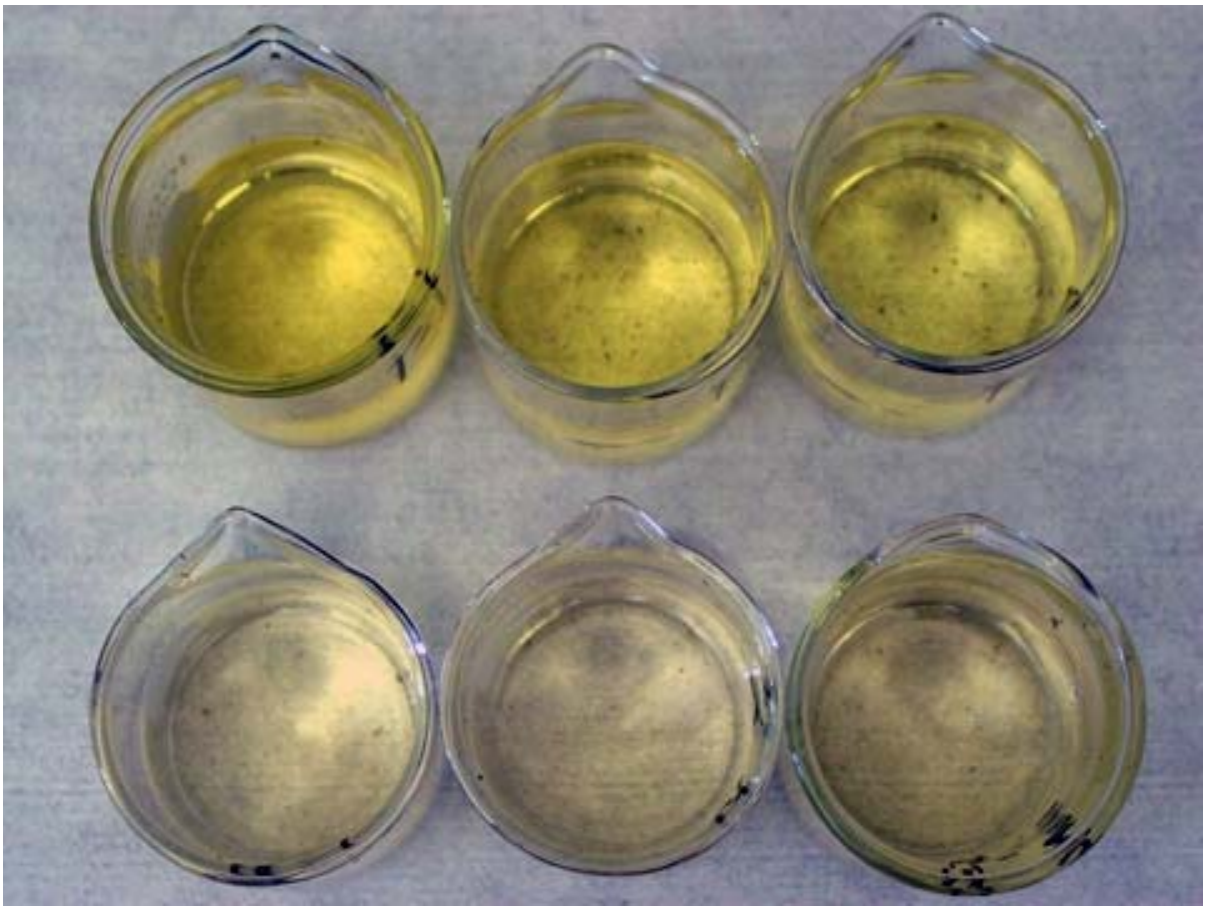

Figure 6.8. Filtrates from "Acid on Demand" preatreatment (top) and conventional pretreatment with H_2SO_4 (bottom). The color associated with the "Acid on Demand" samples is most likely derived from lignin degradation.

These results show that "Acid on Demand" can be more effective at producing fermentable sugars than conventional pretreatments.

6.4 Plasma Flame for Syngas Production

Continuing the focus on alternative fuel sources, the plasma flame was also evaluated as a means of producing syngas ($CO + H_2$). Once formed, syngas can be burned for fuel or

upgraded to higher order liquid fuels via the Fischer-Tropsch process. Conventional processes for syngas synthesis include partial oxidation of coal or methane, and biomass gasification, where biomass feedstocks are heated in oxygen-deficient environments. Given our current dependence on foreign oil and propensity for releasing greenhouse gases, any technique which can generate a domestic fuel in an energy efficient, cost-effective and environmentally friendly manner is of great interest. Since hybrid plasmas are known for their ability to accomplish such goals [18], a feasibility study was carried out to determine whether the plasma flame is capable of producing syngas. Specifically, the plasma flame's propensity for coupling non-equilibrium excitation and gas heating matches the exact requirements of efficient syngas production.

Figure 6.9 shows the partial pressures of various masses as a function of time when reacting CH_4 and H_2O in the plasma flame. The reaction time proceeds from right to left in minutes. Once steady state was reached, i.e. gas flows were stabilized in the reactor and the RGA, the plasma was turned on at 158 kHz and left on for approximately 10 minutes. The driving frequency was then changed to 50 kHz and left on for approximately 2.5 minutes. Changing the frequency effectively changed the discharge's mode of operation such that it became a more thermal discharge (the reason for this behavior was discussed earlier). Thus the reactions took on the characteristics of combustion rather than those associated with non-equilibrium discharges.

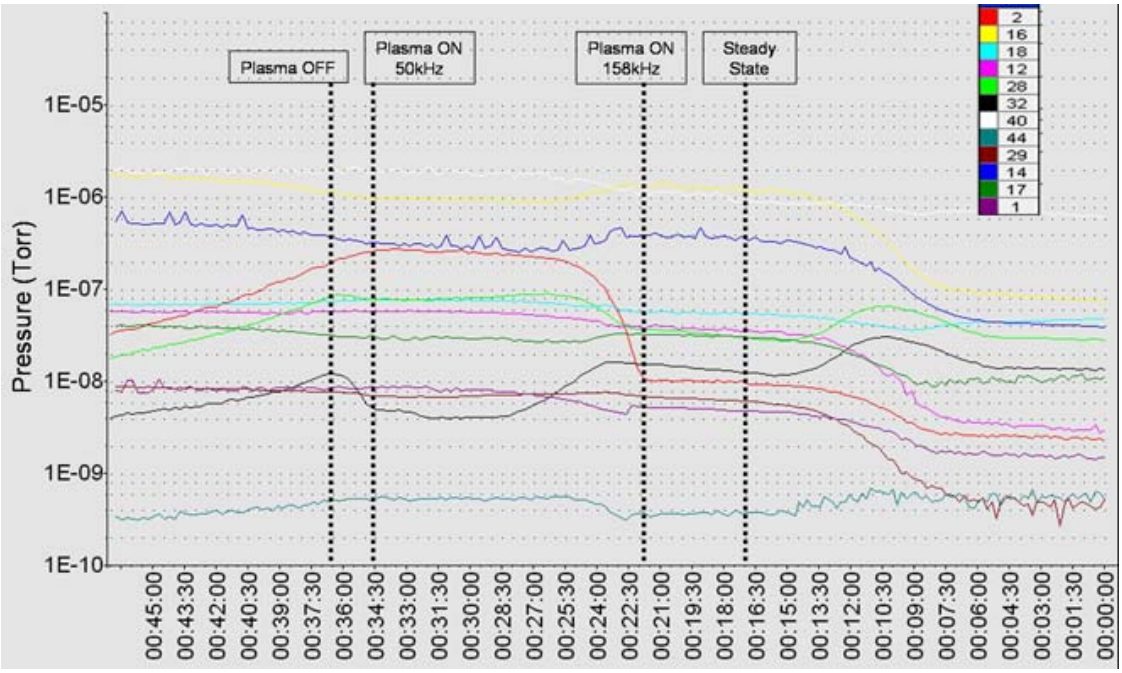

Figure 6.9. RGA results for plasma flame production of syngas. The reaction proceeds in time from right to left and is given in minutes.

When the plasma is ignited at 158 kHz an immediate increase is seen for masses 1, 2 (up 10x) and 28 (up 2x), while a decrease is seen for masses 16, 17, and 32. This can be correlated to the formation of H_2 and CO, and the removal of H_2O and O_2. In other words, the plasma flame is capable of producing syngas from steam and methane. Since this process is only at the feasibility stage, a substantial amount of work is needed to fully evaluate it in terms of efficiency and cost effectiveness.

6.5 Conclusions

Based on the chemical framework of the plasma flame, many applications can be envisioned. As a proof of concept three were presented here; namely, "Acid on Demand" for

both copper etching and production of fermentable sugars, and formation of syngas from CH_4 and H_2O. Positive results were found for each application at a feasibility level. More development will need to take place in order to carry the ideas to commercialization, but this work provides a solid foundation to do so.

7 Concluding Remarks and Future Directions

This work has detailed the development of a hybrid discharge at atmospheric pressure. It was found that the "plasma flame" can produce a gas temperatures and electron densities higher than that of typical non-thermal discharges while still maintaining considerable chemical reactivity.

When using nitrogen and oxygen mixtures as a feed gas, a substantial level of nitrogen dioxide was produced. Upon further investigation, NO_2 synthesis was found to depend primarily on the temperature differential between the plasma and the ambient gas, and also on the population of atomic oxygen. Various process parameters can control these characteristics; of particular importance are applied power and gas mixing ratio. The gas ratio 1N:4O produced the lowest levels of NO_2 and relative O abundance was found to increase linearly with power for this ratio. From this and other observations it was determined that O emission and NO_2 production are negatively dependent on one another. That is, when O is not reacting to form NO_2 it remains in the plasma and is available for excitation and subsequent photon emission; therefore more O emission correlates to less NO_2 production. The gas mixing ratio 4N:1O produced NO_2 at the highest rate and therefore generated the most NO_2 for short reaction times (30 sec, 1 min and 2 min). The mixture 1N:1O had a lower reaction rate, but produced the most NO_2 for longer reaction times (5 min and 10 min). Atomic O emission in both 4N:1O and 1N:1O showed a weak functional dependence, if any dependence at all, on power.

By optimizing the production of NO_2, a process called "Acid on Demand" was created which is able to synthesize nitric acid (HNO_3). This process was then successfully applied to both production of fermentable sugars for bioethanol, and etching of copper for microelectronics. Furthermore, knowledge obtained from studying the nitrogen:oxygen system was applied to a carbon based system (CH_4+H_2O). Reacting this mixture in the plasma flame produced syngas (CO+H_2), which can be used to generate liquid hydrocarbon fuels. Based on these feasibility studies, it is clear that the plasma flame is an extremely useful device with a broad range of potential applicability.

Future investigations relating to experimental characterization of the discharge will involve broadening the power range in which it can be operated. A more in-depth analysis of the chemical species being produced by the plasma flame will also be beneficial. The most significant future work will undoubtedly come in the form of establishing applications for the plasma flame. This could involve further development of the applications presented here, or could be extended to a wide range of topics. Perhaps the most exciting would be developing the plasma flame as a means of generating useful and profitable chemistries from carbon dioxide and other greenhouse gases. This might also include utilizing raw carbon feedstocks as a means of extracting energy from currently unusable waste streams.

8 References

[1] U. Kogelschatz, "Atmospheric-pressure plasma technology," *Plasma Physics and Controlled Fusion*, vol. 46, pp. B63-B75, 2004.

[2] M. Ohring, *The materials science of thin films*, 2nd ed: Academic Press, 2001.

[3] E. E. Kunhardt, "Generation of large-volume, atmospheric-pressure, nonequilibrium plasmas," *Ieee Transactions on Plasma Science*, vol. 28, pp. 189-200, 2000.

[4] U. Kogelschatz, B. Eliasson, and W. Egli, "Dielectric-barrier discharges. Principle and applications," *Journal De Physique Iv*, vol. 7, pp. 47-66, 1997.

[5] U. Kogelschatz, B. Eliasson, and W. Egli, "From ozone generators to flat television screens: history and future potential of dielectric barrier discharges," *Pure Applied Chemistry*, vol. 71, pp. 1819-1828, 1999.

[6] C. Tendero, C. Tixier, P. Tristant, J. Desmaison, and P. Leprince, "Atmospheric pressure plasmas: A review," *Spectrochimica Acta Part B*, vol. 61, pp. 2-30, 2006.

[7] B. Eliasson and U. Kogelschatz, "Nonequilibrium volume plasma chemical processing," *IEEE Transactions on Plasma Science*, vol. 19, pp. 1063-1077, 1991.

[8] A. Fridman, A. Chirokov, and A. Gustol, "Non-thermal atmospheric pressure discharges," *Journal of Physics D-Applied Physics*, vol. 38, pp. R1-R24, 2005.

[9] A. Czernichowski, "Gliding arc. Applications to engineering and environment control," *Pure and Applied Chemistry*, vol. 66, pp. 1301-1310, 1994.

[10] G. Gauglitz and T. Vo-Dinh, "Handbook of Spectroscopy." Weinheim, Germany: Wiley-VCH GmbH & Co. KGaA, 2003.

[11] R. Longhurst, *Geometrical and Physical Optics*, 2nd ed. New York, NY: John Wiley & Sons LTD, 1967.

[12] F. Sears, *Optics*, 3rd ed. Reading, MA: Addison-Wesley Publishing Company, Inc, 1958.

[13] C. Palmer, "Diffraction Gratings: The Crucial Dispersive Element," *Spectroscopy*, vol. 10, pp. 14-15, 1995.

[14] J. Lerner and A. Thevenon, "The Optics of Spectroscopy: A Tutorial," J-Y Optical Systems/ Instruments SA, Inc., Edison, N.J., http://www.horiba.com/us/en/scientific/products/optics-tutorial/?Ovly=1, 1988.

[15] H. Griem, *Spectral Line Broadening by Plasmas*, vol. 39. New York, NY: Academic Press, Inc, 1974.

[16] P. Jansson, *Deconvolution: with applications in spectroscopy*. Orlando, FL: Academic Press, Inc., 1984.

[17] H. Griem, *Plasma Spectroscopy*. New York, NY: McGraw-Hill, Inc., 1964.

[18] A. Fridman, *Plasma Chemistry*. New York: Cambridge University Press, 2008.

[19] J. Luque and D. R. Crosley, "LIFBASE: Database and Spectral Simulation Program (v. 1.5)," *SRI International Report*, 1999.

[20] D. Fletcher, J.-M. Charbonnier, G. S. R. Sarma, and T. Magin, *Physico-Chemical Modeling of High Enthalpy and Plasma Flows*. Rhode-Saint-Genèse, Belgium: The von Karman Institute, 2002.

[21] C. O. Laux, "Radiation and Nonequilibrium Collisional-Radiative Models," in *von Karman Institute Lecture Series*, 2002-2007.

[22] G. Herzberg, *Spectra of Diatomic Molecules*, vol. 1, 2nd ed. New York, NY: Van Nostrand Reinhold Company, 1950.

[23] S. Moon and W. Choe, "A comparative study of rotational temperatures using diatomic OH, O2 and N2+ molecular spectra emitted from atmospheric plasmas," *Spectrochimica Acta Part B*, vol. 58, pp. 249–257, 2003.

[24] J. Stillahn, K. Trevino, and E. Fisher, "Plasma Diagnostics For Unraveling Process Chemistry," *Annual Reviews of Analytical Chemistry*, vol. 1, pp. 261-291, 2008.

[25] H. Griem, *Principles of Plasma Spectroscopy*. Cambridge, UK: Cambridge University Press, 1997.

[26] A. Fridman and L. A. Kennedy, *Plasma Physics and Engineering*. New York: Taylor & Francis, Inc., 2004.

[27] H. Okabe, *Photochemistry of Small Molecules*. New York John Wiley and Sons, 1978.

[28] B. Kirmse, A. Delon, and R. Jost, "NO2 absorption cross section and its temperature dependence," *Journal of Geophysical Research*, vol. 102, pp. 16089-16098, 1997.

[29] R. Ben Gadri, J. R. Roth, T. C. Montie, K. Kelly-Wintenberg, P. P. Y. Tsai, D. J. Helfritch, P. Feldman, D. M. Sherman, F. Karakaya, Z. Y. Chen, and U. T. K. P. S. Team, "Sterilization and plasma processing of room temperature surfaces with a one atmosphere uniform glow discharge plasma (OAUGDP)," *Surface & Coatings Technology*, vol. 131, pp. 528-542, 2000.

[30] M. J. Gallagher, N. Vaze, S. Gangoli, V. N. Vasilets, A. F. Gutsol, T. N. Milovanova, S. Anandan, D. M. Murasko, and A. A. Fridman, "Rapid inactivation of airborne bacteria using atmospheric pressure dielectric barrier grating discharge," *Ieee Transactions on Plasma Science*, vol. 35, pp. 1501-1510, 2007.

[31] Y. Jin, C. S. Ren, Z. L. Xiu, D. Z. Wang, Y. N. Wang, and H. Yu, "Comparison of yeast inactivation treated in He, Air and N-2 DBD plasma," *Plasma Science & Technology*, vol. 8, pp. 720-723, 2006.

[32] M. Laroussi and F. Leipold, "Evaluation of the roles of reactive species, heat, and UV radiation in the inactivation of bacterial cells by air plasmas at atmospheric pressure," *International Journal of Mass Spectrometry*, vol. 233, pp. 81-86, 2004.

[33] M. Laroussi, "Low temperature plasma-based sterilization: Overview and state-of-the-art," *Plasma Processes and Polymers*, vol. 2, pp. 391-400, 2005.

[34] T. C. Montie, K. Kelly-Wintenberg, and J. R. Roth, "An overview of research using the one atmosphere uniform glow discharge plasma (OAUGDP) for sterilization of surfaces and materials," *Ieee Transactions on Plasma Science*, vol. 28, pp. 41-50, 2000.

[35] N. De Geyter, R. Morent, C. Leys, L. Gengembre, and E. Payen, "Treatment of polymer films with a dielectric barrier discharge in air, helium and argon at medium pressure," *Surface & Coatings Technology*, vol. 201, pp. 7066-7075, 2007.

[36] M. Horie, "Plasma-structure dependence of the growth-mechanism of plasma-polymerized fluorocarbon films with residual radicals," *Journal of Vacuum Science & Technology a-Vacuum Surfaces and Films*, vol. 13, pp. 2490-2497, 1995.

[37] F. A. Morsy, S. Y. Elsayad, A. Bakry, and M. A. Eid, "Surface properties and printability of polypropylene film treated by an air dielectric barrier discharge plasma," *Surface Coatings International Part B-Coatings Transactions*, vol. 89, pp. 49-55, 2006.

[38] E. Occhiello, M. Morra, G. Morini, F. Garbassi, and P. Humphrey, "Oxygen-Plasma-Treated Polypropylene Interfaces with Air, Water, and Epoxy-Resins .1. Air and Water," *Journal of Applied Polymer Science*, vol. 42, pp. 551-559, 1991.

[39] X. M. Xie, T. R. Gengenbach, and H. J. Griesser, "Changes in Wettability with Time of Plasme-Modified Perfluorinated Polymers," *Journal of Adhesion Science and Technology*, vol. 6, pp. 1411-1431, 1992.

[40] R. Hackam and H. Akiyama, "Air pollution control by electrical discharges," *Ieee Transactions on Dielectrics and Electrical Insulation*, vol. 7, pp. 654-683, 2000.

[41] H. B. Huang, D. Q. Ye, M. L. Fu, and F. Da Feng, "Contribution of UV light to the decomposition of toluene in dielectric barrier discharge plasma/photocatalysis system," *Plasma Chemistry and Plasma Processing*, vol. 27, pp. 577-588, 2007.

[42] H. J. Kim, C. H. Cho, H. Kim, and S. C. Lee, "Decomposition of carbon tetrachloride in air plasma using glow discharge atomic emission spectrometry," *Analyst*, vol. 123, pp. 607-610, 1998.

[43] Z. Machala, E. Marode, M. Morvova, and P. Lukac, "DC glow discharge in atmospheric air as a source for volatile organic compounds abatement," *Plasma Processes and Polymers*, vol. 2, pp. 152-161, 2005.

[44] T. Oda, T. Takahashi, and K. Tada, "Decomposition of dilute trichloroethylene by nonthermal plasma," *Ieee Transactions on Industry Applications*, vol. 35, pp. 373-379, 1999.

[45] B. M. Penetrante, J. N. Bardsley, and M. C. Hsiao, "Kinetic analysis of non-thermal plasmas used for pollution control," *Japanese Journal of Applied Physics Part 1-Regular Papers Short Notes & Review Papers*, vol. 36, pp. 5007-5017, 1997.

[46] K. Urashima and J. S. Chang, "Removal of volatile organic compounds from air streams and industrial flue gases by non-thermal plasma technology," *Ieee Transactions on Dielectrics and Electrical Insulation*, vol. 7, pp. 602-614, 2000.

[47] J. Van Durme, J. Dewulf, C. Leys, and H. Van Langenhove, "Combining non-thermal plasma with heterogeneous catalysis in waste gas treatment: A review," *Applied Catalysis B-Environmental*, vol. 78, pp. 324-333, 2008.

[48] X. Lu, "Effects of gas temperature and electron temperature on species concentration of air plasmas," *Journal of Applied Physics*, vol. 102, pp. 033302, 2007.

[49] K. U. Becker K H, Schoenbach K H, Barker R J, *Non-equilibrium air plasmas at atmospheric pressure*. London: Institute of Physics Publishing, 2005.

[50] R. Treharne and C. McKibben, "Method and apparatus for home production and application of nitrogen fertilizer," vol. 4,010,897. United States: Charles F. Kettering Foundation, Dayton OH, 1977.

[51] L. Summers, "Process for the synthesis of gases," vol. 1,130,940. United States, 1915.

[52] W. Siebert, "Device for synthesizing gases," vol. 1,073,823. United States, 1913.

[53] F. Du Pont, "Process and apparatus for obtaining oxids of nitrogen from atmospheric air," vol. 1,370,295. United States, 1921.

[54] M. Simek, M. Clupek, B. Vaclav, and P. Sunka, "Production of reactive species by atmospheric pressure streamers in N2-O2 mixtures," *Pure Applied Chemistry*, vol. 78, pp. 1213-1225, 2006.

[55] D.-J. Kim, Y. Choi, and K.-S. Kim, "Effects of process variables on NOx conversion bu pulsed corona discharge process," *Plasma Chemistry and Plasma Processing*, vol. 21, pp. 625-650, 2001.

[56] A. Gentile and M. Kushner, "Reaction chemistry and optimization of plasma remediation of NxOy from gas streams," *Journal of Applied Physics*, vol. 78, pp. 2074-2085, 1995.

[57] Y. Mok and S. Ham, "Conversion of NO to NO2 in air by a pulsed corona discharge process," *Chemical Engineering Science*, vol. 53, pp. 1667-1678, 1998.

[58] G. Zhao, X. Hu, M. Yeung, O. Plumb, and M. Radosz, "Nonthermal plasma reactions of dilute nitrogen oxide mixtures: NOx in nitrogen," *Industrial and Engineering Chemisry Research*, vol. 43, pp. 2315-2323, 2004.

[59] C. McLarnon and V. Mathur, "Nitrogen oxide decomposition by barrier discharge," *Industrial and Engineering Chemisry Research*, vol. 39, pp. 2779-2787
2000.

[60] I. Vinogradov and K. Wiesemann, "Classical absorption and emission spectroscopy of barrier discharges in N2/NO and O2/NOx mixtures," *Plasma Sources Science & Technology*, vol. 6, pp. 307-316, 1997.

[61] K. Yukimura, K. Kawamura, S. Kambara, H. Moritomi, and T. Yamashita, "Correlation of energy efficiency of NO removal by intermittent DBD radical injection method," *IEEE Transactions on Plasma Science*, vol. 33, pp. 763-770, 2005.

[62] E. Willey, "On chemical reaction in the electric discharge II--The synthesis of nitric oxide," *Proceedings of the Royal Society of London. Series A, Mathematical and Physical Sciences*, vol. 159, pp. 247-262, 1937.

[63] J. Westhaver and A. Brewer, "Chemical Action in the Glow Discharge III," *Journal of Physical Chemistry*, vol. 34, pp. 554-562, 1930.

[64] A. Brewer and K. K. PD, "Chemical Action in the Glow Discharge. XI. The Decomposition of Nitrogen Dioxide and the Nitrogen Dioxide Equilibrium.," *Journal of Physical Chemistry*, vol. 37, pp. 889-896, 1933.

[65] L. Henry, "On the Mechanism of the Synthesis of the Nitrogen Oxides," *Journal of Physical Chemistry*, vol. 34, pp. 2782-2791, 1930.

[66] A. Rousseau and L. Gatilova, "NO and NO2 production in pulsed low pressure DC discharge," *Applied Physics Letters*, vol. 86, 2005.

[67] Y. Ionikh, A. Meshchanov, J. Ropcke, and A. Rousseau, "A diode laser study and modeling of NO and NO2 formation in a pulsed DC air discharge," *Chemical Physics*, vol. 322, pp. 411-422, 2006.

[68] J. R. Roth, *Industrial Plasma Engineering: Principles*, vol. 1. London: IOP Publishing, Inc, 1995.

[69] S. Duo, M. Li, Y. Zhou, J. Tong, and G. Sun, "Investigation of surface reaction and degradation mechanism of Kapton during atomic oxygen exposure," *Journal of Materials Science and Technology*, vol. 19, pp. 535-539, 2003.

[70] G. Zhao, M. Argyle, and M. Radosz, "Optical emission study of nonthermal plasma confirms reaction mechanisms involving neutral rather than charged species," *Journal of Applied Physics*, vol. 101, pp. 033303, 2007.

[71] "Estimating Glucose Concentration in Solution," Science and Plants for Schools (SAPS), http://www-saps.plantsci.cam.ac.uk/worksheets/scotland/glucose.htm,

[72] M. Galbe and G. Zacchi, "A review of the production of ethanol from softwood," *Applied Microbiology and Biotechnology*, vol. 59, pp. 618-628, 2002.